Shh$^{floxed/floxed}$ mice were purchased from Jackson Laboratory. We injected each mouse with 8 mg/kg of tamoxifen (Sigma-Aldrich) for 12 consecutive days and produced MI at 7 days after tamoxifen treatment. Because EPOR-null mice are embryonic lethal due to severe anemia, we prepared RES mice expressing EPOR exclusively in the hematopoietic lineage, which were established as described previously (15). EPOR expression is limited to the erythroid lineage cells in the RES mice. The RES mice develop normally and are fertile. GFP transgenic mice were purchased from SLC. Generation and genotyping of dnSTAT3-Tg mice have been previously described (36). Age- and sex-matched WT mice (C57BL/6; SLC) were used as controls. RES mice were provided by M. Yamamoto (Tohoku University School of Medicine, Miyagi, Japan).

Induction of MI and treatment. Mice were anesthetized by intraperitoneal injection of pentobarbital (50 mg/kg) and artificially ventilated with a respirator. Mice were subjected to ligation of the left anterior descending artery or to sham operation as described previously (4). Sham operation was performed by cutting pericardium. EPO (Chugai Pharmaceutical) or the same volume of saline was administered subcutaneously.

Echocardiography. Transthoracic echocardiography was performed with a VisualSonics (Vevo 660; VisualSonics Inc.) equipped with a 25-MHz imaging transducer. Mice were kept awake without anesthesia during the echocardiographic examination to minimize data deviation, and heart rate was approximately 550–650 bpm in all mice.

Histology. Hearts fixed in 10% formalin were embedded in paraffin and sectioned at 4-μm thickness for Masson trichrome staining. Tissue hypoxia was evaluated using the Hypoxyprobe (Chemicon) according to the manufacture's instructions. Fixed frozen sections of the heart samples were immunohistochemically stained by using primary antibodies to PECAM (Pharmingen), dystrophin (Novocastra Laboratories), α-SMA (DAKO), and Mac3 (BD Biosciences). The ischemic area that indicates infarct and border area was measured. For measurement of the cross-sectional area of cardiomyocytes, 50 randomly selected cardiomyocytes in a LV cross-section were measured by tracing dystrophin immunostaining. These measurements were performed with NIH ImageJ software. The samples were stained with Hoechst 33258 (1 μg/ml) or TO-PRO-3 (Molecular Probes Inc.). Immunofluorescence was visualized by laser confocal microscopy (Radiance 2000; Bio-Rad Laboratories).

Bone marrow transplantation. Bone marrow cells were isolated from 8-week-old transgenic mice systemically expressing GFP or WT mice. Bone marrow cells (5×10^7 cells) suspended in 100 μl of PBS containing 3% FBS were injected intravenously into irradiated WT mice or RES mice. A flow cytometric analysis revealed that more 97% of bone marrow cells were derived from donor cells at 6 weeks after bone marrow transplantation.

Flow cytometry. Circulating EPCs derived from bone marrow were detected by flow cytometry using CD34/Flk-1 double labeling. Mice subjected to MI or sham operation were treated with EPO or saline for 3 days subsequent to the operation. Then the mice were sacrificed to collect peripheral blood. The nucleated cells were incubated with FITC-conjugated anti-CD34 monoclonal antibody and PE-conjugated anti-Flk-1 antibody (VEGFR2/KDR; BD Biosciences) for 60 minutes on ice and washed with PBS supplemented with 3% FBS. The labeled nucleated cells were analyzed by the EPICS ALTRA flow cytometer using EXPO32 software (Beckman Coulter).

Western blot analysis. Western blot analysis was performed as described previously (30). Briefly, the infarcted hearts were separated into 2 parts consisting of the ischemic and viable regions. Proteins extracted from the ischemic regions of the infarcted hearts of mice were subjected to SDS-PAGE and then transferred onto polyvinylidene difluoride membranes (GE Healthcare). The membranes were probed using a primary antibody against, Shh-N (5E1; Developmental Studies Hybridoma Bank), VEGF, Patched, GAPDH (Santa Cruz Biotechnology Inc.), Ang-1 (Rockland). and α-tubulin (Sigma-Aldrich). For in vitro study, primary antibodies against Shh, Akt, Bcl-2 (Santa Cruz Biotechnology Inc.), VEGF for rat (R&D systems), phospho-Akt, phospho-ERK, cleaved caspase-3 (Cell Signaling), ERK (Invitrogen), and actin (Sigma-Aldrich) were used. The ECL-plus system (GE healthcare) was used for detection. Coomassie Brilliant Blue (Wako Pure Chemical Industries) was used for staining total protein blot with culture medium supernatant of cardiomyocytes.

In vivo gene transfer. Soluble Flt-1 is known to bind to VEGF, thereby acting on as an inhibitor for VEGF (37). We injected an adenoviral vector encoding the murine soluble *Flt-1* gene (10^9 pfu; Invitrogen) into thigh muscles of mice at 4 days before MI and 3 days after MI. Adenoviral vector encoding LacZ (10^9 PFU) was used as control.

Cell culture. Cardiomyocytes prepared from ventricles of 1-day-old Wistar rats were plated onto 35-mm plastic culture dishes at a concentration of 1×10^5 cells/cm^2 and cultured in DMEM supplemented with 10% FBS at 37°C in a mixture of 95% air and 5% CO_2. The culture medium was changed to serum-free DMEM 24 hours before stimulation. rmShh peptide was purchased from R&D Systems. The plasmid of a truncated form of human EPOR was from Y. Nakamura (RIKEN BioResource Center, Tsukuba, Ibaraki, Japan) (38). Adenoviral vector of truncated EPOR was created using AdEasy Vector System (Qbiogene). Adenoviral vector of dnSTAT3 was a gift from K. Yamauchi-Takihara (Osaka University, Osaka, Japan) (36). siRNA targeting VEGF, Shh, and negative control RNA (Invitrogen) were introduced into rat cardiomyocytes by using Lipofectamine RNAiMAX (Invitrogen) according to the manufacturer's instructions. For immunocytochemical staining, cardiomyocytes and cardiac fibroblasts were cocultured with or without EPO for 48 hours, fixed in 4% paraformaldehyde, and stained with primary antibodies to Shh (Santa Cruz Biotechnology Inc.), α-sarcomeric actinin (Sigma-Aldrich), and vimentin (Progen).

qRT-PCR. qRT-PCR analysis was performed as described previously (39). Total RNA was extracted from sample using the RNeasy kit (QIAGEN). We used 2.5 μg of total RNA to generate cDNA using the Super Script VILO cDNA synthesis kit (Invitrogen). qRT-PCR was carried out on a LightCycler system (Roche) using probes from Universal Probe Library (Roche) and the TaqMan Master Mix (Roche). Sequence of primers and the respective Universal Probe Library probes were as follows: *Ang-1*: forward GGAAGATGGAAGCCTGGAT, reverse ACCAGAGGGATTCCCAAAAC, probe #12; *Gapdh*: forward TGTCCGTCGTGGATCTGAC, reverse CCTGCTTCACCACCTTCTTG, probe #80, each for mouse; *Shh*: forward GAATCCAAAGCTCGCATCC, reverse CAGGTGCACTGTGGCTGAT, probe #38; *Ang-1*: forward GGAAGCCTAGATTTCCAGAGG, reverse ACCAGAGGGATTCCCAAAAC, probe #12; *Ptch-1*: forward CAAAGCTGACTACATGCCAGA, reverse GCGTACTCTATGGGCTCTGC, probe #64, *Gli-1*: forward GGAAGAGAGCAGACTGACTGTG, reverse GGGGAGTGGTCACTGCTG, probe #1; and *Gapdh*: forward AATGTATCCGTTGTGGATCTGA, reverse GCTTCACCACCTTCTTGATGT, probe #80, each for rat. Relative expression of target genes was calculated with the comparative CT method. Each sample was run in duplicate, and the results were systematically normalized using *Gapdh*.

Apoptosis analysis. Frozen sections of the heart samples and cultured cardiomyocytes fixed by 4% paraformaldehyde were subjected to TUNEL staining using a commercially available kit (In Situ Apoptosis Detection Kit; Takara Biomedicals) as directed by manufacturer. Annexin V-Cy3 Apoptosis Detection Kit (BioVision) was used to detect apoptotic cardiomyocytes according to the manufacture's instructions. Cultured cardiomyocytes were serum starved in DMEM with 0.5% FBS and treated with EPO (10 U/ml) or normal saline for 8 hours prior to beginning H_2O_2 (100 μM) treatment. Cyclopamine (40-42) (5 μM), LY294002 (5 μM), and PD98059 (10 μM; Calbiochem) were administered 15 minutes before EPO treatment.

DNA synthesis assay. DNA synthesis was measured by performing a BrdU incorporation assay with a commercially available kit (Roche) as directed by the manufacturer. Cardiomyocyte-conditioned medium was collected as previously described (43). Briefly, cultured cardiomyocytes were starved in DMEM without FBS and were pretreated with EPO (10 U/ml) or saline for 48 hours, and then the medium was collected and transferred to HUVECs. HUVECs were plated in 96-well plates at a density of 5×10^4 cells/well in endothelial cell basal medium-2 with EGM-2 Bullet Kit (Cambrex) for 8 hours and then switched to cardiomyocyte-conditioned medium for 12 hours. BrdU was added to the medium, and BrdU incorporation was detected by ELISA using anti-BrdU antibody. VEGF receptor antagonist CBO-P11 (44, 45) (12 μM; Calbiochem) and anti-Ang-1 antibody (1 μg/ml; Chemicon) were used for the inhibition studies.

Tube formation assay. Matrigel (growth factor reduced, 100 μl; BD Biosciences) was added to each well of a 48-well plate and allowed to polymerize at 37°C for 1 hour. HUVECs (1×10^4) were seeded onto Matrigel in endothelial cell basal medium-2 with EGM-2 Bullet Kit and cultured for 1 hour and then switched to cardiomyocyte-conditioned medium described above. After 8 hours, tube length was quantified using an angiogenesis image analyzer (Kurabo).

Isolated heart perfusion system. Isolated heart perfusion system was used to measure coronary flow as previously described (46). In brief, mouse hearts were excised rapidly and mounted on a Langendorff perfusion system. All isolated hearts were stabilized by perfusion of Krebs-Henseleit buffer, and perfusion pressure was adjusted to 60 mmHg. The heart was paced at 400 bpm. After an adjustment period, the coronary effluent was collected and the coronary flow was calculated. After baseline measurements, sodium nitroprusside (10^{-4} M, Sigma-Aldrich) was infused into the perfusate, and coronary flow was measured.

Statistics. All data are shown as mean ± SEM. Multiple group comparison was performed by 1-way ANOVA followed by Bonferroni's procedure for comparison of means. Comparison between 2 groups was analyzed by the 2-tailed Student's *t* test. Values of $P < 0.05$ were considered statistically significant.

Acknowledgments

The authors thank M. Yamamoto (Tohoku University School of Medicine, Miyagi, Japan) for generously providing RES mice. The authors thank Y. Ohtsuki, M. Ikeda, I. Sakamoto, A. Furuyama, M. Kikuchi, and H. Maruyama for their excellent technical assistance. This work was supported by a Grant-in-Aid for Scientific Research from the Ministry of Education, Science, Sports, and Culture, and Health and Labor Sciences research grants (to I. Komuro) and a Grant-in-Aid for Scientific Research from the Ministry of Education, Culture, Sports, Science and Technology of Japan and grants from the Terumo Life Science Foundation (to H. Takano).

Received for publication May 18, 2009, and accepted in revised form March 24, 2010.

Address correspondence to: Issei Komuro, Department of Cardiovascular Science and Medicine, Chiba University Graduate School of Medicine, 1-8-1 Inohana, Chuo-ku, Chiba 260-8670, Japan. Phone: 81.43.226.2097; Fax: 81.43.226.2557; E-mail: komuro-tky@umin.ac.jp.

1. Jessup M, Brozena S. Heart failure. *N Engl J Med.* 2003;348(20):2007–2018.
2. Rosamond W, et al. Heart disease and stroke statistics--2008 update: a report from the American Heart Association Statistics Committee and Stroke Statistics Subcommittee. *Circulation.* 2008;117(4):e25–146.
3. Moon C, et al. Erythropoietin reduces myocardial infarction and left ventricular functional decline after coronary artery ligation in rats. *Proc Natl Acad Sci U S A.* 2003;100(20):11612–11617.
4. Ohtsuka M, et al. Cytokine therapy prevents left ventricular remodeling and dysfunction after myocardial infarction through neovascularization. *FASEB J.* 2004;18(7):851–853.
5. Harada M, et al. G-CSF prevents cardiac remodeling after myocardial infarction by activating the Jak-Stat pathway in cardiomyocytes. *Nat Med.* 2005;11(3):305–311.
6. Silverberg DS, et al. The effect of correction of mild anemia in severe, resistant congestive heart failure using subcutaneous erythropoietin and intravenous iron: a randomized controlled study. *J Am Coll Cardiol.* 2001;37(7):1775–1780.
7. Ponikowski P, et al. Effect of darbepoetin alfa on exercise tolerance in anemic patients with symptomatic chronic heart failure: a randomized, double-blind, placebo-controlled trial. *J Am Coll Cardiol.* 2007;49(7):753–762.
8. Felker GM, Adams KF Jr, Gattis WA, O'Connor CM. Anemia as a risk factor and therapeutic target in heart failure. *J Am Coll Cardiol.* 2004;44(5):959–966.
9. Bahlmann FH, et al. Erythropoietin regulates endothelial progenitor cells. *Blood.* 2004; 103(3):921–926.
10. Parsa C, et al. A novel protective effect of erythropoietin in the infarcted heart. *J Clin Invest.* 2003; 112(7):999–1007.
11. Wright GL, Hanlon P, Amin K, Steenbergen C, Murphy E, Arcasoy MO. Erythropoietin receptor expression in adult rat cardiomyocytes is associated with an acute cardioprotective effect for recombinant erythropoietin during ischemia-reperfusion injury. *FASEB J.* 2004;18(9):1031–1033.
12. Brines M, Cerami A. Emerging biological roles for erythropoietin in the nervous system. *Nat Rev Neurosci.* 2005;6(6):484–494.
13. Tada H, et al. Endogenous erythropoietin system in non-hematopoietic lineage cells plays a protective role in myocardial ischemia/reperfusion. *Cardiovasc Res.* 2006;71(3):466–477.
14. Asaumi Y, et al. Protective role of endogenous erythropoietin system in nonhematopoietic cells against pressure overload-induced left ventricular dysfunction in mice. *Circulation.* 2007;115(15):2022–2032.
15. Suzuki N, et al. Erythroid-specific expression of the erythropoietin receptor rescued its null mutant mice from lethality. *Blood.* 2002;100(7):2279–2288.
16. Li Y, et al. Reduction of inflammatory cytokine expression and oxidative damage by erythropoietin in chronic heart failure. *Cardiovasc Res.* 2006;71(4):684–694.
17. Hirose S, et al. Erythropoietin attenuates the development of experimental autoimmune myocarditis. *Cardiovasc Drugs Ther.* 2007;21(1):17–27.
18. Abbate A, Biondi-Zoccai GG, Baldi A. Pathophysiologic role of myocardial apoptosis in post-infarction left ventricular remodeling. *J Cell Physiol.* 2002;193(2):145–153.
19. Latini R, Brines M, Fiordaliso F. Do non-hemopoietic effects of erythropoietin play a beneficial role in heart failure? *Heart Fail Rev.* 2008;13(4):415–423.
20. Pagès G, Pouysségur J. Transcriptional regulation of the Vascular Endothelial Growth Factor gene--a concert of activating factors. *Cardiovasc Res.* 2005;65(3):564–573.
21. Wang L, et al. The sonic hedgehog pathway mediates carbamylated erythropoietin-enhanced proliferation and differentiation of adult neural progenitor cells. *J Biol Chem.* 2007;282(42):32462–32470.
22. Pola R, et al. The morphogen sonic hedgehog is an indirect angiogenic agent upregulating two families of angiogenic growth factors. *Nat Med.* 2001;7(6):706–711.
23. Kusano KF, et al. Sonic hedgehog myocardial gene therapy: tissue repair through transient reconstitution of embryonic signaling. *Nat Med.* 2005;11(11):1197–1204.
24. Washington Smoak I, et al. Sonic hedgehog is required for cardiac outflow tract and neural crest cell development. *Dev Biol.* 2005;283(2):357–372.
25. Lewis PM, et al. Cholesterol modification of sonic hedgehog is required for long-range signaling activity and effective modulation of signaling by Ptc1. *Cell.* 2001;105(5):599–612.
26. Sohal DS, et al. Temporally regulated and tissue-specific gene manipulations in the adult and embryonic heart using a tamoxifen-inducible Cre protein. *Circ Res.* 2001;89(1):20–25.
27. Suri C, et al. Increased vascularization in mice overexpressing angiopoietin-1. *Science.* 1998; 282(5388):468–471.
28. Asahara T, et al. Tie2 receptor ligands, angiopoietin-1 and angiopoietin-2, modulate VEGF-induced postnatal neovascularization *Circ Res.* 1998;83(3):233–240.
29. Holash J, Wiegand SJ, Yancopoulos GD. New model of tumor angiogenesis: dynamic balance between vessel regression and growth mediated by angiopoietins and VEGF. *Oncogene.* 1999;18(38):5356–5362.
30. Sano M, et al. p53-induced inhibition of Hif-1 causes cardiac dysfunction during pressure overload. *Nature.* 2007;446(7134):444–448.
31. Giordano FJ, et al. A cardiac myocyte vascular endothelial growth factor paracrine pathway is required to maintain cardiac function. *Proc Natl Acad Sci U S A.* 2001;98(10):5780–5785.
32. Lavine KJ, Kovacs A, Ornitz DM. Hedgehog signaling is critical for maintenance of the adult coronary vasculature in mice. *J Clin Invest.* 2008;118(7):2404–2414.
33. Androutsellis-Theotokis A, et al. Notch signaling regulates stem cell numbers in vitro and in vivo. *Nature.* 2006;442(7104):823–826.
34. Kasperczyk H, Baumann B, Debatin KM, Fulda S. Characterization of sonic hedgehog as a novel

NF-kappaB target gene that promotes NF-kappaB-mediated apoptosis resistance and tumor growth in vivo. *FASEB J.* 2009;23(1):21–33.
35. Digicaylioglu M, Lipton SA. Erythropoietin-mediated neuroprotection involves cross-talk between Jak2 and NF-kappaB signalling cascades. *Nature.* 2001;412(6847):641–647.
36. Funamoto M, et al. Signal transducer and activator of transcription 3 is required for glycoprotein 130–mediated induction of vascular endothelial growth factor in cardiac myocytes. *J Biol Chem.* 2000;275(14):10561–10566.
37. Kendall RL, Thomas KA. Inhibition of vascular endothelial cell growth factor activity by an endogenously encoded soluble receptor. *Proc Natl Acad Sci U S A.* 1993;90(22):10705–10709.
38. Nakamura Y, Komatsu N, Nakauchi H. A truncated erythropoietin receptor that fails to prevent programmed cell death of erythroid cells. *Science.* 1992;257(5073):1138–1141.
39. Leucht C, Stigloher C, Wizenmann A, Klafke R, Folchert A, Bally-Cuif L. MicroRNA-9 directs late organizer activity of the midbrain-hindbrain boundary. *Nat Neurosci.* 2008;11(6):641–648.
40. Taipale J, et al. Effects of oncogenic mutations in Smoothened and Patched can be reversed by cyclopamine. *Nature.* 2000;406(6799):1005–1009.
41. Berman D, et al. Medulloblastoma growth inhibition by hedgehog pathway blockade. *Science.* 2002;297(5586):1559–1561.
42. Watkins DN, Berman DM, Burkholder SG, Wang B, Beachy PA, Baylin SB. Hedgehog signalling within airway epithelial progenitors and in small-cell lung cancer. *Nature.* 2003;422(6929):313–317.
43. Zhang Y, Pasparakis M, Kollias G, Simons M. Myocyte-dependent regulation of endothelial cell syndecan-4 expression. Role of TNF-alpha. *J Biol Chem.* 1999;274(8):4786–4790.
44. Zilberberg L, et al. Structure and inhibitory effects on angiogenesis and tumor development of a new vascular endothelial growth inhibitor. *J Biol Chem.* 2003;278(37):35564–35573.
45. Heineke J, et al. Cardiomyocyte GATA4 functions as a stress-responsive regulator of angiogenesis in the murine heart. *J Clin Invest.* 2007;117(11):3198–3210.
46. Bendall J, et al. C. Strain-dependent variation in vascular responses to nitric oxide in the isolated murine heart. *J Mol Cell Cardiol.* 2002;34(10):1325–1333.

MOLECULAR AND CELLULAR BIOLOGY, Mar. 2011, p. 1054–1065 Vol. 31, No. 5
0270-7306/11/$12.00 doi:10.1128/MCB.00732-10

Increased Akt-mTOR Signaling in Lung Epithelium Is Associated with Respiratory Distress Syndrome in Mice[▽]

Hiroyuki Ikeda,[1,2] Ichiro Shiojima,[1,3] Toru Oka,[1,3] Masashi Yoshida,[1] Koji Maemura,[4] Kenneth Walsh,[5] Takashi Igarashi,[2] and Issei Komuro[1,3]*

Department of Cardiovascular Science and Medicine, Chiba University Graduate School of Medicine, Chiba, Japan[1]; Department of Pediatrics, University of Tokyo Graduate School of Medicine, Tokyo, Japan[2]; Department of Cardiovascular Medicine, Osaka University Graduate School of Medicine, Suita, Japan[3]; Department of Cardiovascular Medicine, Nagasaki University Graduate School of Biomedical Sciences, Nagasaki, Japan[4]; and Molecular Cardiology, Whitaker Cardiovascular Institute, Boston University School of Medicine, Boston, Massachusetts[5]

Received 24 June 2010/Returned for modification 31 August 2010/Accepted 17 December 2010

Pregnancy in women with diabetes is associated with a higher risk of perinatal complications. In particular, infants of diabetic mothers frequently suffer from respiratory distress syndrome (RDS), which is a leading cause of death in preterm infants and is considered to be primarily due to hyperinsulinemia in infants in response to maternal hyperglycemia. To elucidate the mechanism of how insulin signaling induces RDS, bronchoalveolar epithelium-specific Akt1 transgenic (TG) mice were generated. Akt1 overexpression in fetal lung epithelium resulted in RDS in preterm infants born by Caesarean section at embryonic day 18.5 (E18.5). The expression levels of hypoxia-inducible factor 2α (HIF-2α) and its target vascular endothelial growth factor (VEGF) were downregulated in the lung of Akt1 TG mice. Inhibition of the Akt-mammalian target of rapamycin (mTOR) signaling axis by rapamycin restored the expression of VEGF and improved the lung pathology of Akt1 TG pups. Rapamycin also attenuated the RDS phenotype in wild-type mice delivered preterm at E17.5. In cultured lung epithelial cells, insulin reduced VEGF expression and transcriptional activity of HIF-2 on *VEGF* promoter in an mTOR-dependent manner. Thus, aberrant activation of the Akt-mTOR pathway in lung epithelium plays a causal role in the pathogenesis of infant RDS, presumably through downregulation of HIF-2-dependent VEGF expression in the lung.

Pregnancy in women with diabetes is associated with a higher risk of perinatal complications. The estimated prevalence rate of gestational diabetes is approximately 4% and is considered to represent 90% of all cases of diabetes diagnosed during pregnancy (2). Moreover, pregnant women with type 2 diabetes are increasing in number in line with the rapid increase in the prevalence of type 2 diabetes in all age groups (9). Infants of diabetic mothers frequently suffer from macrosomia, neonatal hypoglycemia, cardiomegaly, respiratory difficulties, and other congenital anomalies (3, 5, 14, 21), which are considered to be primarily due to hyperinsulinemia in infants in response to maternal hyperglycemia. Respiratory distress syndrome (RDS) is one of the most clinically significant perinatal complications, with high morbidity and mortality (19, 22). RDS is caused by attenuated production of pulmonary surfactant, a mixture of phospholipids and surfactant-associated proteins that covers the alveolar surface and prevents alveolar collapse by reducing the surface tension of the air-water interface (12). Because pulmonary surfactant is specifically produced by type II lung epithelial cells, attenuated production of pulmonary surfactant is considered to be due to impaired differentiation and/or maturation of type II lung epithelial cells (31). Reduced expression of surfactant-associated proteins was observed in fetuses of streptozotocin-induced diabetic rats or in insulin-treated human fetal lung explants (8, 10, 11), suggesting that hyperactivation of insulin signaling in the lung plays a causal role in the pathogenesis of RDS of infants having a diabetic mother.

Phosphatidylinositol 3-kinase (PI3K) is activated by insulin and is responsible for most of the metabolic actions of insulin. PI3K also controls cell growth, differentiation, survival, and protein synthesis (28). The involvement of the PI3K pathway in RDS was suggested by a previous report showing that bronchoalveolar-specific deletion of *Pten* in mice led to upregulation of the PI3K pathway in the lung and resulted in RDS associated with marked hyperplasia of alveolar epithelial cells, increased numbers of bronchoalveolar stem cells (BASCs), and impaired production of surfactant proteins (SPs) (33). It was also shown that genetic ablation of hypoxia-inducible factor 2α (HIF-2α) causes RDS due to downregulation of vascular endothelial growth factor (VEGF) expression in the lung and that intratracheal VEGF administration stimulates maturation of type II lung epithelial cells (4). However, the downstream effectors of PI3K that cause RDS and the mechanistic link between the PI3K pathway and HIF-2-dependent VEGF expression in the lung have been elusive.

Using bronchoalveolar epithelium-specific Akt1 transgenic (TG) mice, we show here that aberrant activation of the Akt-mammalian target of rapamycin (mTOR) pathway in lung epithelium plays a causal role in the pathogenesis of infant RDS. We also provide evidence suggesting that sustained Akt-mTOR activation induces RDS through downregulation of HIF-2-dependent VEGF expression in the lung.

* Corresponding author. Mailing address: Department of Cardiovascular Medicine, Osaka University Graduate School of Medicine, 2-2 Yamadaoka, Suita 565-0871, Japan. Phone: 81 6 6879 3631. Fax: 81 6 6879 3639. E-mail: komuro-tky@umin.ac.jp.

▽ Published ahead of print on 28 December 2010.

MATERIALS AND METHODS

Animals and DOX administration. SP-C-rtTA TG mice expressing the reverse tetracycline transactivator (rtTA) protein under the control of the human surfactant protein-C promoter (pro-SP-C) on the FVB/N background were de-

scribed previously (23, 29) and were purchased from the Jackson Laboratory. These mice were crossed with Tet-myrAkt1 TG mice (25) harboring a myristoylated Akt1 (myrAkt1) transgene under the control of multimerized *tetO* sequences maintained on a mixed background of FVB/N, C57BL/6J, and 129Sv. For myrAkt1 expression, dams were treated with doxycycline (DOX) in drinking water from embryonic day 0.5 (E0.5) at a final concentration of 0.5 mg/ml (25, 29). Respiratory rate was measured by visual inspection of the movements of thorax and abdomen for 1 min. All animal procedures were performed with the approval of the Institutional Animal Care and Use Committee of Chiba University.

Histological analysis and immunohistochemistry. Lungs were formalin fixed without constant pressure inflation and embedded in paraffin for histological analyses. Serial sections of 4 μm were stained with hematoxylin and eosin (HE) for morphological analysis, periodic acid-Schiff (PAS) for detection of glycogen-rich cells, and Masson's trichrome (MT) for detection of fibrosis. Aerated lung area and alveolar septal thickness were measured in toluidine blue-stained sections using ImageJ software (4). Aerated lung area was measured in 10 visual fields for each animal. Septal thickness was measured at 10 points in each visual field, and 10 visual fields for each animal were used for the measurement. The size and number of saccules were measured in PAS-stained sections using ImageJ software. The size of 10 saccules was measured in each visual field, and 10 visual fields for each animal were used for the analysis. Saccular number was counted in 10 visual fields for each animal. Immunohistochemistry was performed using an avidin-biotin-horseradish peroxidase detection system with Ni-diaminobenzidine (DAB) (ABC kit; Vector Laboratories) and Nuclear Fast Red as a counterstain. The antibodies used were hemagglutinin (HA), pro-SP-C, Clara cell 10-kDa protein (CC10), aquaporin-5 (AQP5), VEGF (Santa Cruz Biotechnology), and calcitonin gene-related peptide (CGRP; BioMol).

Fluorescence imaging. A BZ-9000 (Keyence) microscope was used for fluorescence imaging. Paraffin-embedded lung sections were incubated with isolectin B4-fluorescein isothiocyanate (FITC) conjugate (Sigma) to detect endothelial cells and with wheat germ agglutinin-tetramethyl rhodamine isothiocyanate (TRITC) conjugate (Sigma) to counterstain the cell membrane. Vascular cell counts with three replications were performed with BZ application software (Keyence), and the median value was used for each sample.

Western blot analysis. Total protein lysate was extracted from lung tissue, and SDS-PAGE was performed as described previously (26). The antibodies used were HA, total Akt1, total S6 kinase (S6K), SP-A, pro-SP-C, AQP5, CC10, VEGF, glyceraldehyde-3-phosphate dehydrogenase (GAPDH; Santa Cruz Biotechnology), phospho-Akt (Ser473), phospho-S6K1 (Thr389), phospho-S6 (Ser235/236), total S6, phospho-glycogen synthase kinase 3β (phospho-GSK3β) (Ser9), phospho-FOXO3a (318/321), total FOXO3a (Cell Signaling Technology), SP-B, SP-D (Chemicon/Millipore), and HIF-2α (Novus Biologicals). Densitometric analysis was performed using ImageJ.

Mouse model of preterm infants. Pups were collected by Caesarean section at E18.5 for Akt1 TG mice and at E17.5 for wild-type ICR mice (4, 20). The umbilical cord was cut, amniotic fluid and membranes were removed from the mouth and nose, and body temperature was kept at 37°C.

Administration of rapamycin. Rapamycin (LC Laboratories) was prepared in the solvent containing 0.2% sodium carboxymethylcellulose and 0.25% polysorbate-80 in water (24, 25). Rapamycin (1 mg/kg of body weight/day) or vehicle was administered subcutaneously to dams.

Reporter gene assays. Luciferase assays were performed essentially as previously described (18). The plasmids used were VEGF reporter plasmid (pGL2hVEGF) and the expression vectors for HIF-1α (phHIF-1α), HIF-2α (phEP-1), and ARNT (phARNT). A549 cells were transfected with the plasmids indicated in the Fig. 8 legend and treated with 250 μM $CoCl_2$ to mimic hypoxic condition.

Statistical analysis. Data are expressed as means ± standard errors of the means (SEM). Statistical significance between two groups was determined with a Student's *t* test or χ^2 test. Probability values of <0.05 were considered to be statistically significant.

RESULTS

Generation of bronchoalveolar epithelium-specific Akt1 TG mice. Two lines of TG mice (Tet-myrAkt1 and SP-C-rtTA) were used to generate bronchoalveolar epithelium-specific Akt1 TG mice (Fig. 1A). The Tet-myrAkt1 TG line harbors an active form of the Akt1 transgene (myrAkt1) under the control of multimerized tetracycline operator (*tetO*) sequences (25), and the SP-C-rtTA TG line expresses the reverse tetracycline transactivator (rtTA) in respiratory epithelial cells driven by human surfactant protein-C (SP-C) promoter (23, 29). DOX enables rtTA binding to *tetO* sequences by inducing its conformational change. Therefore, DOX treatment of double-TG (DTG) mice harboring both transgenes induces transcription of the myrAkt1 gene in lung epithelial cells (Fig. 1A). Mating of SP-C-rtTA mice with Tet-myrAkt1 mice resulted in the generation of mice with four different genotypes (wild type, Tet-myrAkt1 single TG, SP-C-rtTA single TG, and DTG) at the expected frequencies. Western blot analysis of lung lysates harvested at postnatal day 0 (P0) revealed that the transgene product detected by anti-HA blotting was observed in the lung of DTG mice treated with DOX (Fig. 1B). The induced expression of myrAkt1 was associated with a marked increase in phosphorylation levels of several downstream effectors such as S6K1, S6, and glycogen synthase kinase-3 (GSK3), but not FOXO3 (Fig. 1B). Because it was reported that treatment of SP-C-rtTA mice with DOX may exert toxic effects on alveolar epithelial cells (20), the phenotype of DOX-treated SP-C-rtTA single-TG mice was carefully compared with littermates of other genotypes (wild type, Tet-myrAkt1 single TG, and DTG). However, although there was an obvious lung phenotype in DTG mice (described in detail below), no apparent abnormality was observed in mice with other genotypes under our experimental conditions (Fig. 1C and D). We therefore used DOX-treated single-TG littermates as controls in this study.

Akt activation in lung epithelial cells *in utero* results in transient tachypnea associated with delayed maturation of the lung. Activation of Akt signaling in the lung was achieved by DOX treatment of dams starting at embryonic day 0.5 (E0.5). When analyzed at P0, DTG pups were viable and exhibited no cyanosis or growth retardation (Fig. 2A). Postnatal growth of DTG animals was also comparable to that of control mice. However, DTG mice at P0 exhibited significant tachypnea (Fig. 2B) and various histological abnormalities such as markedly reduced aerated space, increased atelectasis, bronchiolar hyperplasia, impaired thinning of the alveolar septa, and abundant PAS-positive glycogen stores (Fig. 2C to E). Since PAS-positive glycogen is normally converted to surfactant phospholipids in mature epithelial cells, these observations suggest that the differentiation of lung epithelial cells is impaired by aberrant activation of Akt signaling. Of note, these histological findings were improved spontaneously at P2 (Fig. 2C to E). Although mild elastic fiber deposition was observed at P2, no such pathology was evident at the age of 12 weeks (data not shown). Thus, Akt activation in lung epithelium induces transient respiratory difficulties associated with lung maturational defects, which improves spontaneously after birth.

Akt activation in lung epithelial cells *in utero* results in increased numbers of CC10/SP-C double-positive cells and defective maturation of lung epithelial cells. In order to further assess the extent of epithelial differentiation, we performed Western bolt analysis of surfactant proteins (SP-A to SP-D) and immunohistochemistry of marker proteins: SP-C for type II alveolar epithelial cells, Clara cell 10-kDa protein (CC10) for Clara cells, aquaporin-5 (AQP5) for type I alveolar epithelial cells, and calcitonin gene-related peptide (CGRP) for neuroendocrine cells. Western blot analysis of surfactant proteins revealed downregulation of SP-B and upregulation of

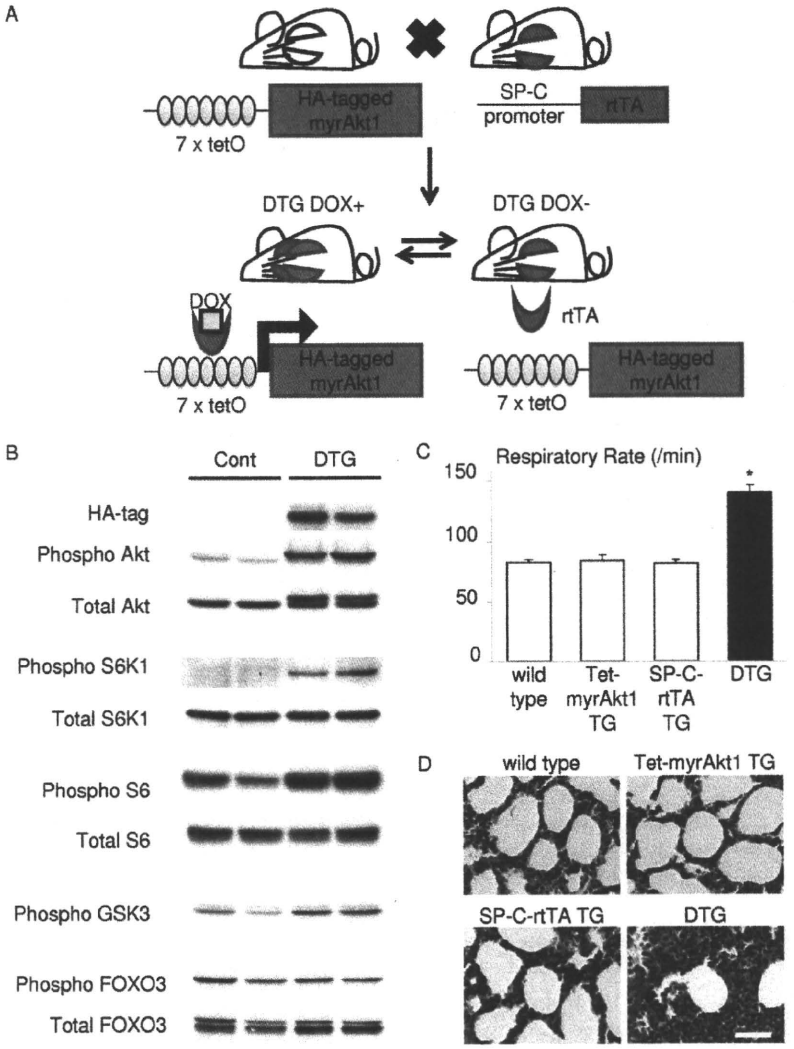

FIG. 1. Generation of bronchoalveolar epithelium-specific Akt1 TG mice. (A) Schematic illustration of binary TG system. (B) Western blot analysis of the whole-lung lysate from control and DTG mice at P0. (C) Respiratory rate at P0. DOX-treated SP-C-rtTA TG mice do not show respiratory distress. *, $P < 0.05$ versus DOX-treated wild-type, Tet-myrAkt1 TG mice, and SP-C-rtTA TG mice (n = 7, 5, 6, and 6 mice, respectively, from 3 dams). All animals were treated with DOX in the drinking water. (D) HE staining of the lung sections. Scale bar, 50 μm.

SP-D, whereas the expression levels of SP-A and SP-C were not altered (Fig. 3A). Western blot analysis and immunohistochemistry also revealed increased expression of CC10 and reduced expression of AQP5 in the lung of DTG mice (Fig. 3A and B). CGRP expression was not altered between control and DTG mice (date not shown). Previous studies characterized CC10/SP-C double-positive cells as BASCs that reside at the bronchoalveolar duct junction and differentiate to both Clara cells and type II alveolar epithelial cells; the latter further differentiate to type I alveolar epithelial cells (15). Double immunostaining revealed that CC10/SP-C double-positive cells were increased in number in the lung of DTG mice (Fig. 3C and D). Collectively, these findings suggest that aberrant activation of Akt signaling in lung epithelial cells results in increased numbers of CC10/SP-C double-positive cells and impaired differentiation of alveolar epithelial cells.

Akt activation in lung epithelial cells *in utero* results in RDS in preterm infants. Since RDS is more frequent in preterm infants than in full-term infants, we examined preterm infants born by Caesarean section at E18.5. DTG mice born at E18.5 showed cyanosis (Fig. 4A) associated with an irregular respiratory pattern, and all DTG mice died by 2 h after birth (Fig. 4B). The airway spaces of DTG lungs were filled with amorphous, proteinaceous material that was not observed in control lungs (Fig. 4C). PAS staining revealed that the size and the density of saccules in DTG lung were smaller and higher than those of controls, respectively (Fig. 4D to F). Western blot analysis of surfactant proteins revealed downregulation of SP-B, whereas the expression levels of SP-A, -C, and -D were not altered (Fig. 4G). Immunohistochemistry also revealed expansion of CC10/SP-C double-positive cells in the lung of DTG mice (Fig. 4H to J). AQP5 expression was barely detect-

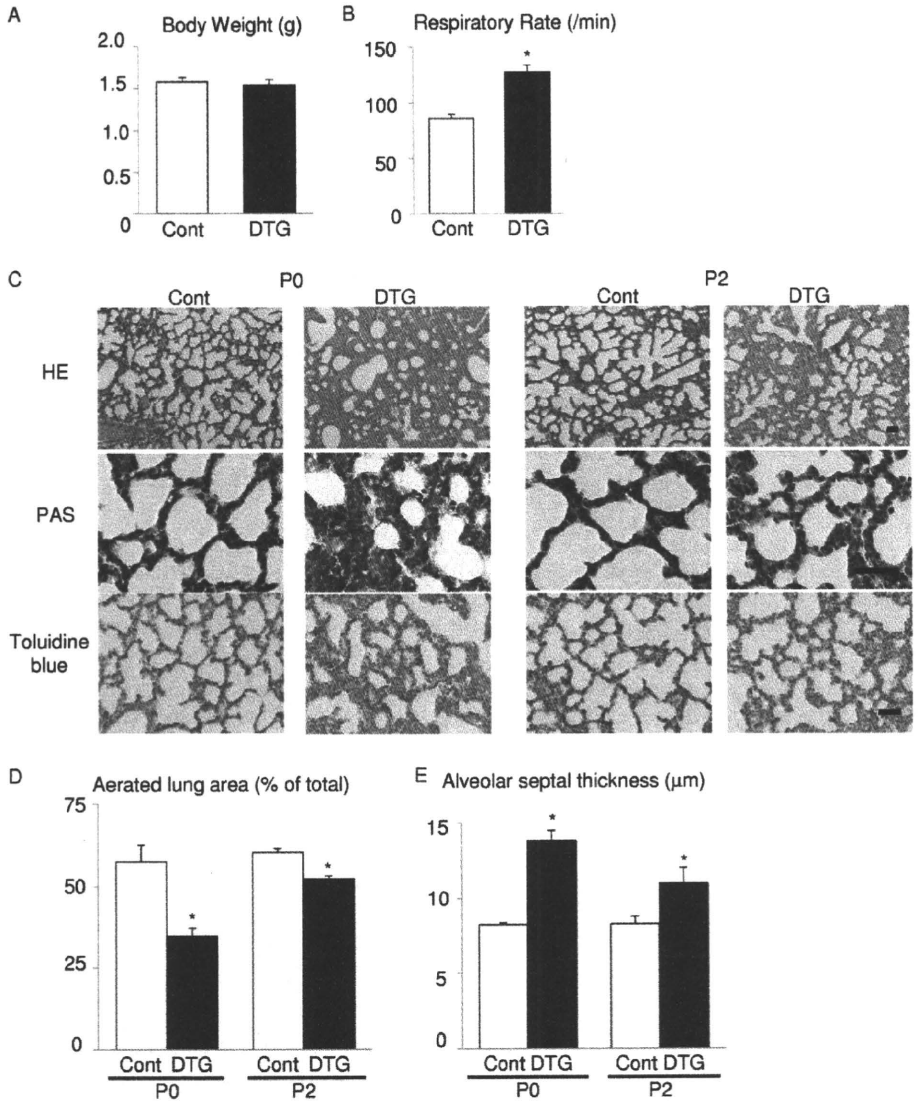

FIG. 2. Akt activation in lung epithelium induces tachypnea and delayed maturation of the lung. (A) Body weight at P0 of control (Cont; $n = 6$) and DTG ($n = 4$) mice from 2 dams. (B) Respiratory rate at P0 of control ($n = 14$) and DTG ($n = 8$) mice from 4 dams. (C) Histological analysis. HE, PAS, and toluidine blue staining of lung sections at P0 and P2. Scale bar, 50 mm. (D) Aerated lung area in control and DTG mice at P0 and P2. *, $P < 0.05$ versus control. (E) Thickness of alveolar septum in control and DTG mice at P0 and P2. *, $P < 0.05$ versus control. For experiments shown in panels D and E, $n = 3$ from a single dam under all conditions.

able at this stage (data not shown). These results collectively suggest that Akt activation in lung epithelial cells *in utero* results in RDS and perinatal lethality in preterm infants.

Rapamycin improves respiratory distress and lung maturational defects induced by Akt1 overexpression in lung epithelium. To test whether the Akt-mTOR pathway mediates lung pathology in DTG mice, rapamycin was administered to dams for 3 days (at E17.5, E18.5, and E19.5). Downregulation of mTOR signaling by rapamycin was confirmed by reduced phosphorylation levels of S6K1 (Fig. 5A). Examination of infants at P0 demonstrated that tachypnea observed in vehicle-treated DTG mice was improved by rapamycin treatment (Fig. 5B). Hematoxylin and eosin (HE) staining revealed that abnormal morphology of lung alveoli in DTG mice was reversed by rapamycin treatment (Fig. 5C, upper panel), and PAS staining demonstrated a reduced number of PAS-positive glycogen stores following rapamycin treatment (Fig. 5C, lower panel). By quantitative analysis of toluidine blue-stained sections, a decrease in aerated space and an increase in alveolar septal thickness observed in DTG mice were rescued by rapamycin treatment (Fig. 5D and E). Impaired differentiation of lung epithelial cells in DTG mice was also improved by rapamycin treatment, as evidenced by reduced expression of CC10, increased expression of AQP5, and a normal expression pattern of SP-C (Fig. 5F). These results suggest that mTOR is critically involved

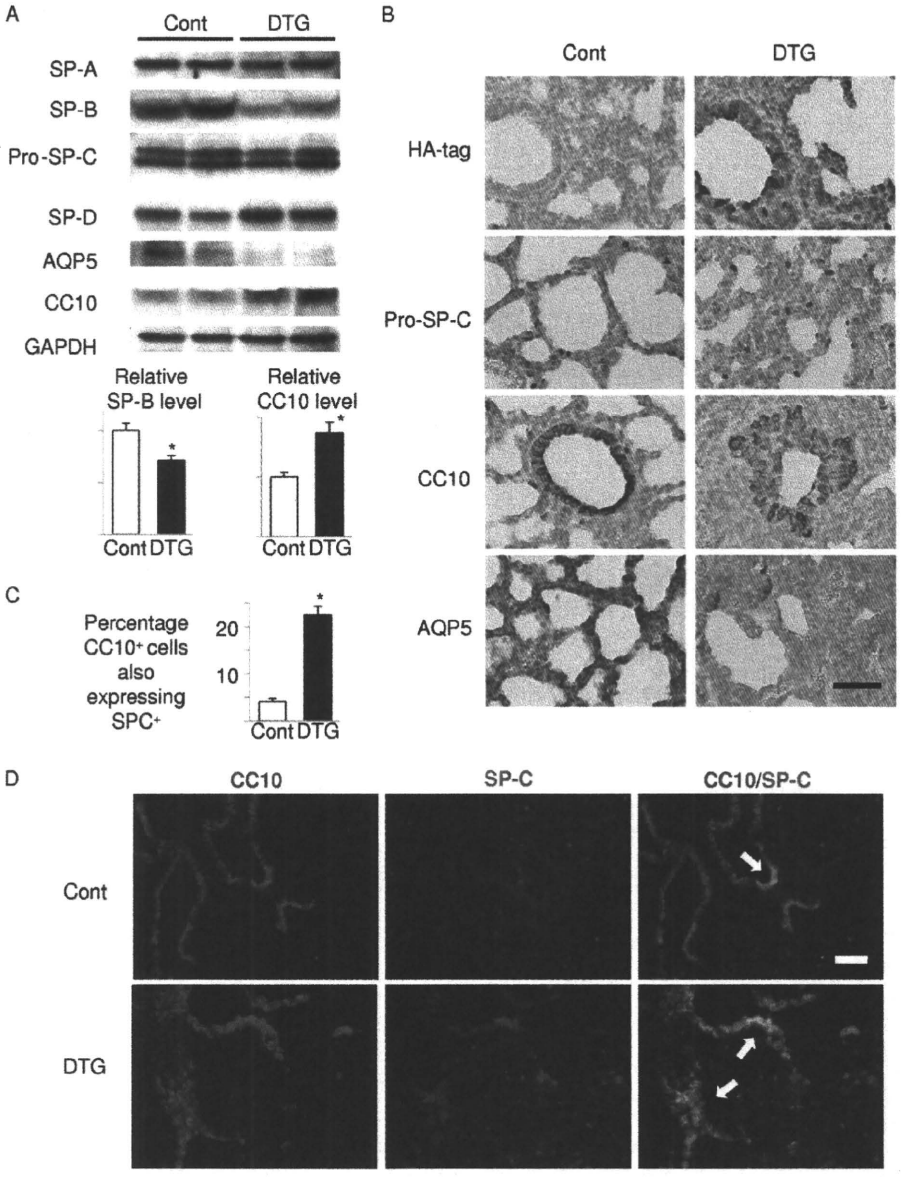

FIG. 3. Akt activation in lung epithelium results in defective maturation of lung epithelial cells and expansion of CC10/SP-C double-positive cells. (A) Western blot analysis of surfactant proteins (SP-A, SP-B, pro-SP-C, and SP-D), CC10 (a marker of Clara cells), and AQP5 (a marker of type I alveolar cells). Lower panels show densitometric analysis. *, $P < 0.05$ versus control ($n = 4$ mice from 2 dams for both controls and DTG). (B) Immunohistochemical analysis of HA tag (Akt1 transgene), SP-C, CC10, and AQP5. SP-C, CC10, and AQP5 were detected in cuboidal type II alveolar cells, Clara cells, and flat type I alveolar cells, respectively. Scale bar, 50 μm. (C and D). Double immunostaining of CC10 and SP-C. CC10/SP-C double-positive cells are indicated by arrows. Scale bar, 100 μm. *, $P < 0.05$ versus control ($n = 5$ control and $n = 3$ DTG mice from 3 dams).

in respiratory distress and lung maturational defects induced by Akt1 overexpression in lung epithelium.

Rapamycin improves respiratory distress induced by preterm delivery. The above-mentioned results suggest the possibility that mTOR activation mediates RDS in wild-type infants delivered preterm. To test this hypothesis, pregnant wild-type mice were treated with vehicle or rapamycin at E15.5 and E16.5, and pups were collected at E17.5 by Caesarean section. Inhibition of mTOR in the lung of rapamycin-treated pups was confirmed by reduced phosphorylation levels of S6K1 (Fig. 6A). All pups delivered from vehicle-treated dams died within 1 h after birth, whereas more than 50% of pups delivered from rapamycin-treated dams survived in this time frame (Fig. 6B). Histological examination revealed that rapamycin treatment promoted lung maturation, as demonstrated by increased aerated lung area, decreased alveolar septal wall thickness, a normal expression pattern of SP-C, and increased expression of AQP5 (Fig. 6C to F). Thus, downregulation of mTOR signal-

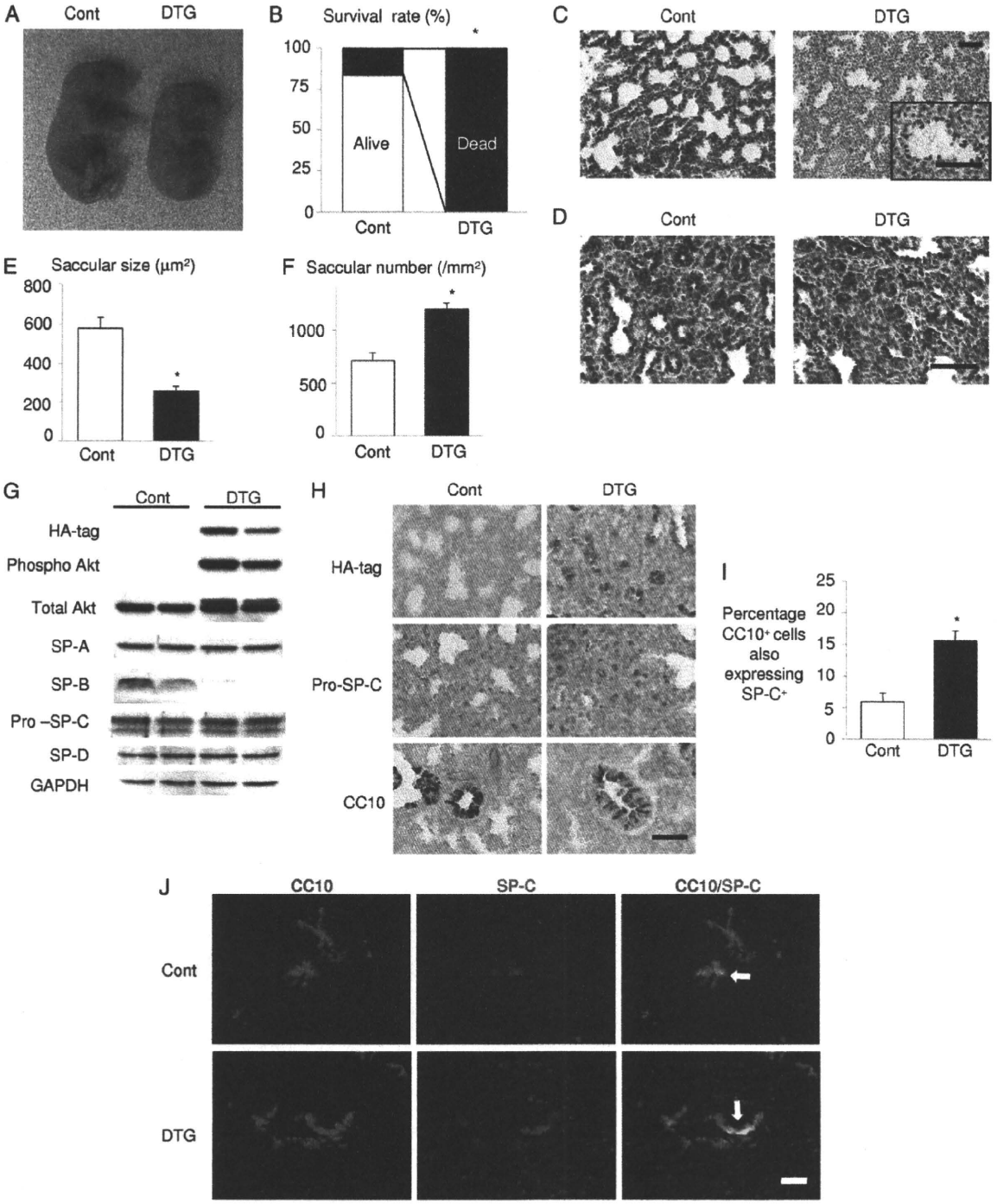

FIG. 4. Akt activation in lung epithelium results in RDS and lethality in preterm infants. (A) Gross appearance of infants. (B) Survival rate by 2 h after delivery. *, $P < 0.05$ ($n = 6$ control and $n = 5$ DTG mice from 2 dams). (C) HE staining of the lung sections of infants delivered by Caesarean section at E18.5. Scale bar, 50 μm. (D) PAS staining of the lung sections of infants delivered by Caesarean section at E18.5. Scale bar, 50 μm. (E) Saccular size at E18.5. *, $P < 0.05$ versus control. (F) Saccular number at E18.5. *, $P < 0.05$ versus control. For the experiments shown in panels E and F, $n = 3$ control and $n = 4$ DTG mice from 2 dams. (G) Western blot analysis of surfactant proteins (SP-A, SP-B, pro-SP-C, and SP-D). (H) Immunohistochemistry of HA tag (Akt1 transgene), pro-SP-C, and CC10 at E18.5. Scale bar, 50 μm. (I and J) Double immunostaining of CC10 and SP-C. CC10/SP-C double-positive cells are indicated by arrows. Scale bar, 100 μm. For both panels, $n = 4$ (Cont) and $n = 3$ (DTG) from 2 dams.

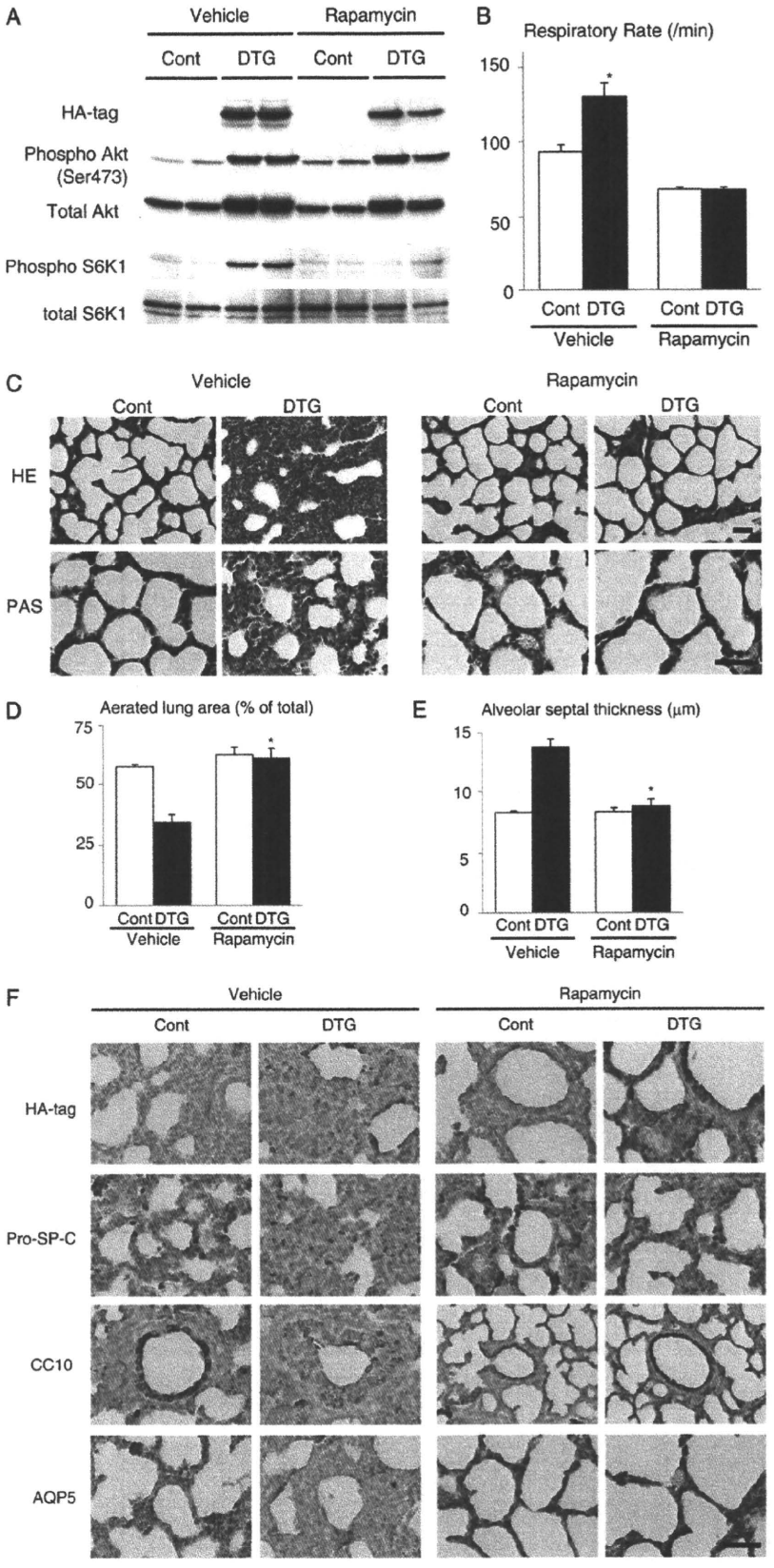
A
Vehicle
Rapamycin
Cont
DTG
Cont
DTG
HA-tag
Phospho Akt (Ser473)
Total Akt
Phospho S6K1
total S6K1
B
Respiratory Rate (/min)
150
100
50
0
*
Cont DTG
Cont DTG
Vehicle
Rapamycin
C
Vehicle
Rapamycin
Cont
DTG
Cont
DTG
HE
PAS
D
Aerated lung area (% of total)
75
50
25
0
*
Cont DTG
Cont DTG
Vehicle
Rapamycin
E
Alveolar septal thickness (μm)
15
10
5
0
*
Cont DTG
Cont DTG
Vehicle
Rapamycin
F
Vehicle
Rapamycin
Cont
DTG
Cont
DTG
HA-tag
Pro-SP-C
CC10
AQP5

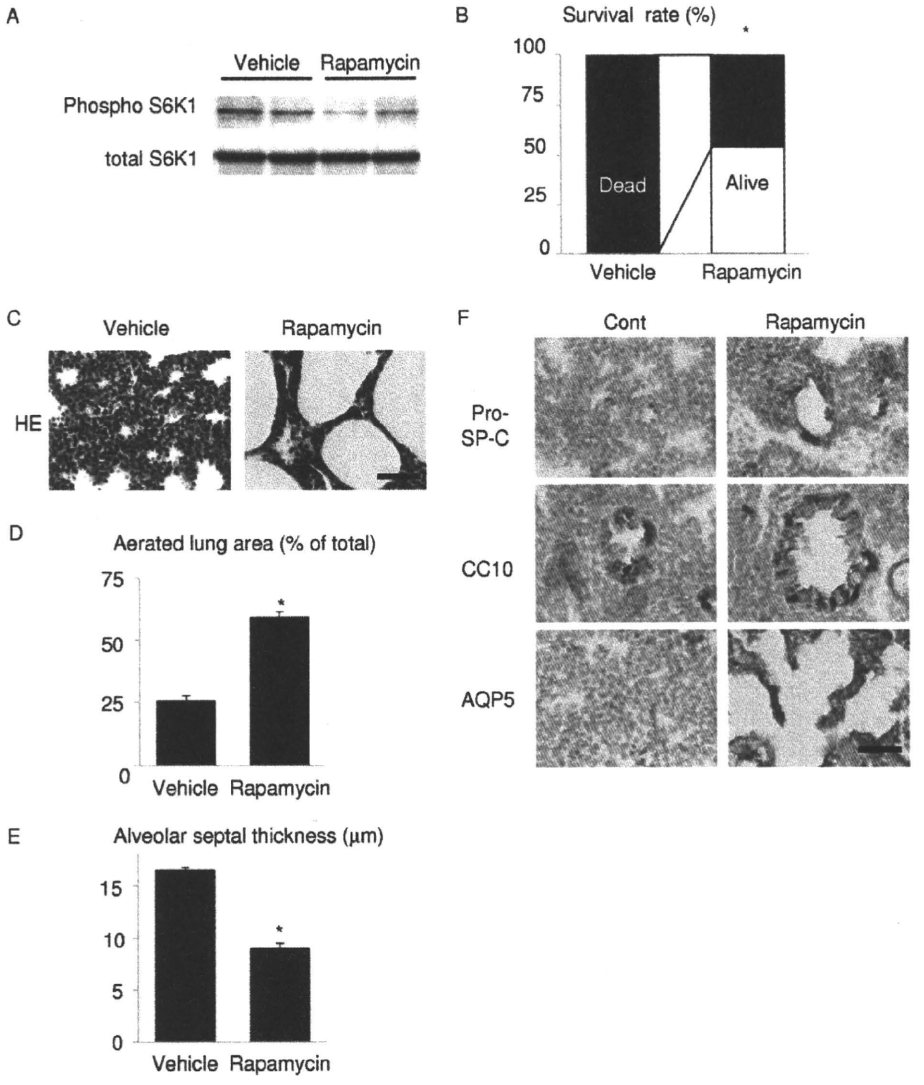

FIG. 6. Rapamycin improves respiratory distress and lung maturational defects induced by preterm delivery. (A) Western blot analysis of S6K1 in the lung. (B) Survival rate of wild-type pups 1 h after Caesarean section at E17.5. *, $P < 0.05$ versus vehicle-treated group. In the vehicle-treated group, $n = 15$ from a single dam. In the rapamycin group, $n = 24$ from 2 dams. (C) HE staining at 1 h after delivery. Scale bar, 50 μm. (D) Aerated lung area in vehicle- or rapamycin-treated pups. *, $P < 0.05$ versus vehicle-treated group. In the vehicle-treated group, $n = 3$ from a single dam; in the rapamycin group, $n = 4$ from 2 dams. (E) Thickness of alveolar septum in vehicle- or rapamycin-treated pups. *, $P < 0.05$ versus vehicle-treated group. In the vehicle-treated group, $n = 3$ from a single dam; in the rapamycin group, $n = 4$ from 2 dams. (F) Immunohistochemistry of pro-SP-C, CC10, and AQP5. Scale bar, 50 μm.

ing has a therapeutic potential for RDS induced by preterm delivery in wild-type mice.

Activation of the Akt-mTOR pathway attenuates HIF-2-dependent VEGF expression in lung epithelial cells. To investigate the mechanism by which Akt-mTOR signaling affects lung maturation, we examined the expression of VEGF, an angiogenic growth factor that is produced in the distal airway during late gestation and regulates coordinated development of alve-

FIG. 5. Rapamycin improves respiratory distress and lung maturational defects induced by Akt1 overexpression in lung epithelium. (A) Western blot analysis of Akt and S6K1 in the lung. (B) Respiratory rate of vehicle- or rapamycin-treated pups at P0. For vehicle experiments, $n = 7$ for both control and DTG mice from 3 dams; for rapamycin experiments, $n = 14$ (control) and $n = 11$ (DTG) mice from 4 dams. (C) Histological analysis. HE and PAS staining of lung sections at P0. Scale bar, 50 μm. (D) Aerated lung area in vehicle- or rapamycin-treated pups at P0. *, $P < 0.05$ versus vehicle-treated DTG mice. (E) Thickness of alveolar septum in vehicle- or rapamycin-treated pups at P0. *, $P < 0.05$ versus vehicle-treated DTG mice. For experiments shown in panels D and E, $n = 3$ control and $n = 3$ DTG vehicle-treated mice from 3 dams, and $n = 8$ control and $n = 7$ DTG rapamycin-treated mice from 4 dams. (F) Immunohistochemistry of HA tag, pro-SP-C, CC10, and AQP5 at P0. Scale bar, 50 μm.

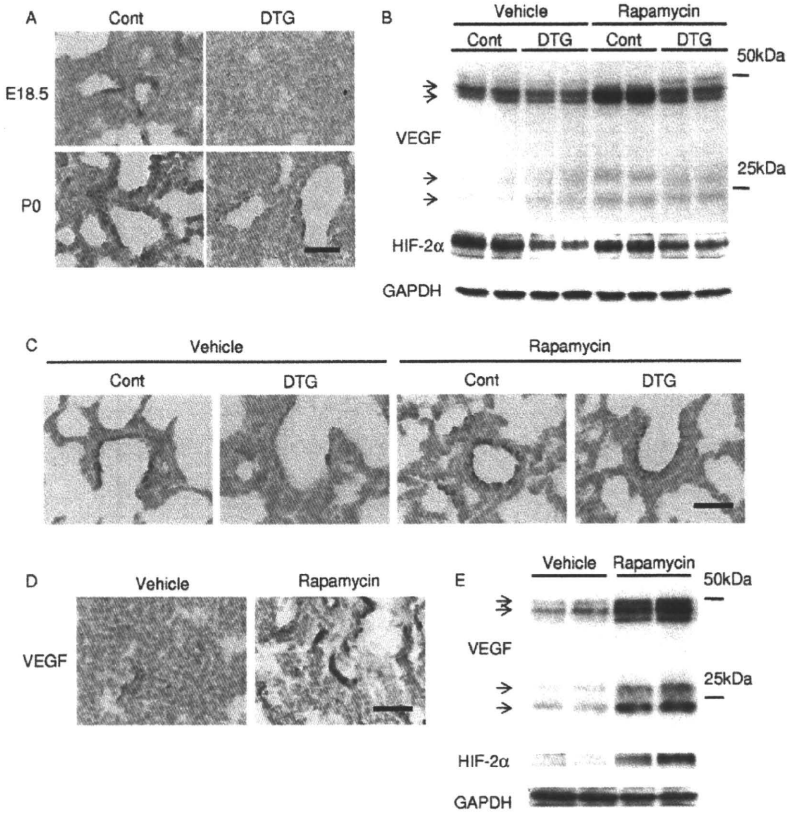

FIG. 7. Akt-mTOR pathway downregulates VEGF expression in the lung. (A) Immunostaining of VEGF at E18.5 and P0 in Akt1 TG mice. Scale bar, 50 μm. (B) Western blot analysis of VEGF and HIF-2α at P0 in Akt1 TG mice. (C) Immunostaining of VEGF at P0 in Akt1 TG mice. Scale bar, 50 μm. (D) Immunostaining of VEGF at E17.5 in wild-type mice. Scale bar, 50 μm. (E) Western blot analysis of VEGF and HIF-2α at E17.5 in wild-type mice.

olar epithelium and capillaries (4). Immunohistochemistry and Western blot analysis revealed that the expression levels of VEGF were downregulated in DTG mice both at E18.5 and P0 and were restored by rapamycin treatment (Fig. 7A to C). Since the expression of VEGF in the lung has been reported to depend on HIF-2 activity (4), we next examined the expression of HIF-2α protein in the lung. Western blot analysis revealed that the HIF-2α protein amount was downregulated in the lung of DTG mice (Fig. 7B). The expression levels of VEGF and HIF-2α were also examined in vehicle- or rapamycin-treated wild-type pups delivered at E17.5. Immunohistochemistry and Western blot analysis demonstrated the upregulation of VEGF and HIF-2α expression by rapamycin in wild-type mice delivered preterm (Fig. 7D and E). It was therefore concluded that activation of the Akt-mTOR pathway attenuates the expressions of VEGF and HIF-2α in the lung. However, it was also noted that the expression levels of HIF-2α do not necessarily correlate with those of VEGF because rapamycin treatment highly upregulated VEGF expression in control animals without altering HIF-2α expression levels (Fig. 7B, compare the vehicle control group and the rapamycin control group). We therefore examined whether Akt-mTOR signaling regulates the transcriptional activity of HIF-2. In cultured A549 lung epithelial cells, insulin induced downregulation of VEGF expression, which was reversed by rapamycin treatment (Fig. 8A). Luciferase assays using *VEGF-luc* as a reporter gene revealed that insulin attenuated transcriptional activity of HIF-2 on VEGF promoter, which was reversed by rapamycin treatment (Fig. 8B), while both insulin and rapamycin had minimal effects on HIF-1 transcriptional activity (Fig. 8C). These results suggest that activation of Akt-mTOR signaling attenuates HIF-2-dependent VEGF expression with respect to both the amount of HIF-2α protein and HIF-2 transcriptional activity.

Activation of the Akt-mTOR pathway reduces alveolar capillary density. To test whether Akt-mTOR-mediated downregulation of VEGF is associated with attenuated alveolar angiogenesis, vascular morphometry was performed in DTG and control mice at P0. Isolectin B4 staining revealed that alveolar capillary density was significantly reduced in DTG mice compared to that in control mice, and this reduction was rescued by rapamycin treatment (Fig. 9A and B). We also found that alveolar capillary density in wild-type mice delivered preterm at E17.5 was increased by rapamycin treatment (Fig. 9C and D). Thus, alveolar capillary density is closely linked to the level of VEGF expression in the lung. These results are consistent with our hypothesis that Akt-mTOR signaling promotes RDS through downregulation of VEGF.

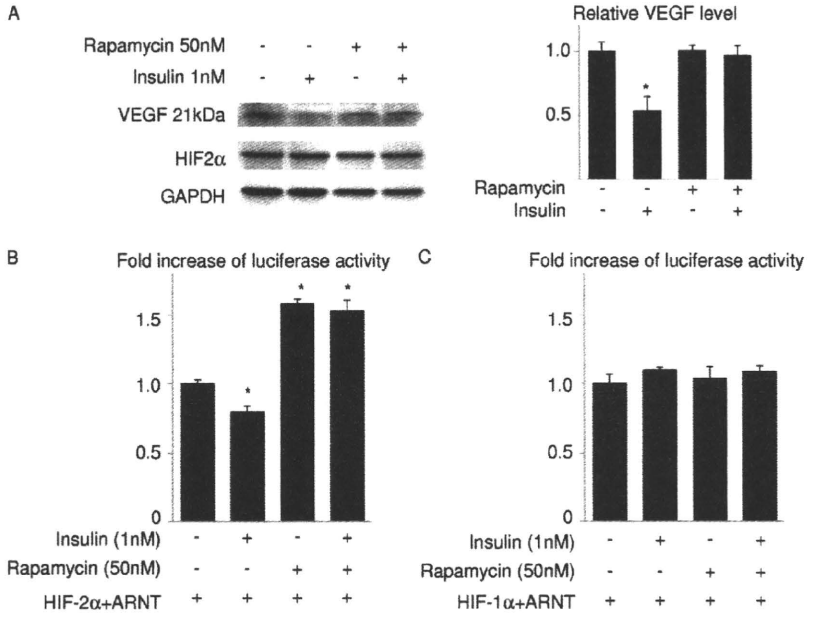

FIG. 8. Insulin attenuates VEGF expression and HIF-2 transcriptional activity on *VEGF* promoter in an mTOR-dependent manner in lung epithelial cells. (A) Western blot analysis of VEGF and HIF-2α in A549 cells treated with insulin and/or rapamycin for 48 h. The right panel shows the densitometric analysis. *, $P < 0.05$ versus the rapamycin (−)/insulin (−) group ($n = 3$ for each group). (B and C) Luciferase assays in A549 cells. A549 cells were transfected with a *VEGF-luc* reporter and expression vectors for HIF-1α, HIF-2α, and ARNT and treated with insulin and/or rapamycin. All experiments were performed in the presence of $CoCl_2$ to mimic hypoxic conditions. *, $P < 0.05$ versus the rapamycin (−)/insulin (−) group.

DISCUSSION

In this study we have demonstrated that activation of Akt signaling in lung epithelial cells during embryogenesis results in transient respiratory difficulties in full-term infants and in RDS in preterm infants. These respiratory defects were associated with bronchiolar hyperplasia, expansion of CC10/SP-C double-positive cells, and impaired maturation of lung epithelial cells. We also found that Akt-mTOR signaling is critically involved in the pathogenesis of RDS because rapamycin treatment improved respiratory distress and lung maturational defects induced by Akt activation or preterm delivery. Mechanistically, Akt-mTOR signaling attenuates both the protein amounts and transcriptional activity of HIF-2, leading to downregulation of HIF-2-dependent expression of VEGF, an angiogenic growth factor that is required for maturation of alveolar epithelial cells. These observations suggest the possibility that aberrant activation of Akt-mTOR signaling or preterm delivery before the appropriate downregulation of this signaling axis plays a causal role in RDS through downregulation of HIF-2-dependent VEGF expression and that the mTOR-HIF-2 pathway may be a novel therapeutic target for infant RDS.

RDS is frequently observed in infants of diabetic mothers, and hyperactivation of insulin signaling in response to maternal hyperglycemia has been proposed to play a pathogenic role (19, 22). It was also previously shown that alveolar epithelium-specific deletion of *Pten* results in RDS, with approximately 90% of neonates dying within 2 h after birth (33). This phenotype of conditional *Pten* deletion is more severe than that of alveolar epithelium-specific Akt1 transgenic mice, suggesting the possibility that PI3K-dependent but Akt-independent pathways are also implicated in the occurrence of RDS. However, because another line of lung epithelium-specific *Pten* knockout mice generated by a similar method exhibit a very mild phenotype (i.e., lack of neonatal lethality, normal postnatal development, and mild bronchiolar hyperplasia) (7), the variation of phenotypes among different animal models may be due in part to the differences in the genetic background of the animals. Furthermore, rapamycin treatment of dams significantly improved the phenotype of alveolar epithelium-specific Akt1 transgenic mice. Taken together, these observations suggest that activation of the PI3K-Akt-mTOR pathway in lung epithelial cells *in utero* plays a causal role in the pathogenesis of RDS in infants with diabetic mothers.

Lung development in mice is histologically divided into four phases: the pseudoglandular stage (E9.5 to 16.5), canalicular stage (E16.5 to 17.5), terminal sac stage (E17.5 to P5), and alveolar stage (P5 to P30) (30). Differentiation of type I and type II epithelial cells and high levels of Pten expression in respiratory epithelium occur at the terminal sac stage (17), which is consistent with the idea that downregulation of the PI3K-Akt-mTOR pathway is required for epithelial differentiation. In humans, lung development is relatively advanced compared with that of mice, and the terminal sac stage corresponds to human preterm infants between 26 and 36 weeks of gestation, when a high complication rate of RDS is observed. Thus, inhibition of the PI3K-Akt-mTOR pathway at specific time points during a later stage of embryogenesis appears to be critical for normal lung development and maturation, and aberrant activation of Akt-mTOR signaling or preterm delivery

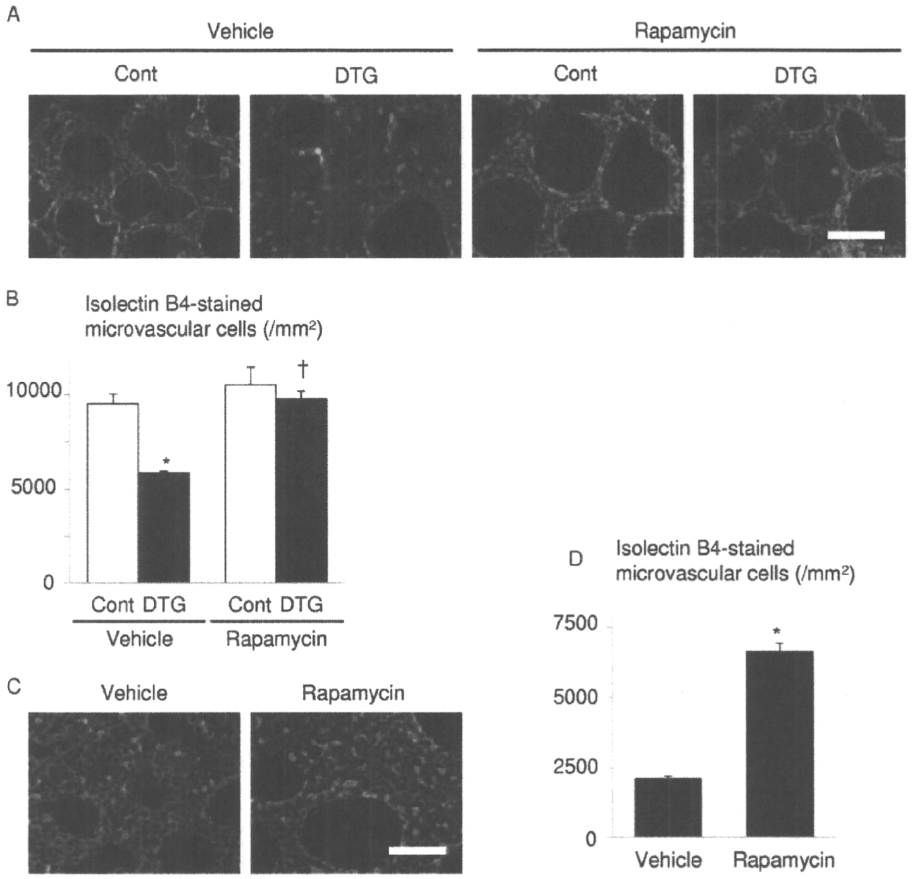

FIG. 9. Alveolar capillary bed formation is impaired by Akt1 overexpression in lung epithelium, which is improved by rapamycin administration to the dams. (A) Histological analysis of vehicle- or rapamycin-treated pups at P0. Sections were stained with isolectin B4-FITC conjugate (green) to detect endothelial cells and with wheat germ agglutinin-TRITC conjugate (red) for membrane staining. Scale bar, 50 μm. (B) Alveolar capillary density. *, $P < 0.05$ versus vehicle-treated control mice; †, $P < 0.05$ versus vehicle-treated DTG mice. In the vehicle-treated group, $n = 4$ control and $n = 3$ DTG mice from 2 dams; in the rapamycin group, $n = 4$ control and $n = 4$ DTG mice from 2 dams. (C) Histological analysis of vehicle- or rapamycin-treated wild-type pups born by Caesarean section at E17.5. Scale bar, 50 μm. (D) Alveolar capillary density. *, $P < 0.05$ versus vehicle-treated mice ($n = 4$ vehicle-treated mice from a single dam, and $n = 4$ rapamycin-treated mice from 2 dams).

before this signaling pathway is appropriately downregulated may result in the occurrence of RDS. The observation that rapamycin was effective for RDS also suggests that downregulation of mTOR signaling is sufficient to induce maturation of lung epithelial cells. Previous studies also implicated GATA6-Wnt/β-catenin signaling and calcineurin/nuclear factor of activated T cells (NFAT) signaling in lung maturation (6, 34). How these two signaling pathways and the PI3K-Akt-mTOR pathway coordinately regulate normal lung development remains to be investigated. It should also be noted that VEGF-induced angiogenesis is enhanced in the presence of rapamycin, which is inconsistent with the observation that VEGF induces endothelial cell proliferation via the Akt-mTOR pathway (32). This may be in part explained by the proangiogenic effects of the rapamycin-insensitive downstream effectors of Akt such as glycogen synthase kinase-3 and the FOXO family of transcription factors (1, 16).

Epithelial-endothelial interactions during lung development are critical in establishing a functional blood-gas interface, and normal lung function depends on the coordinated development of alveolar epithelium and capillaries, which is primarily regulated by VEGF (27). It was previously shown that deletion of HIF-2α in mice causes RDS due to downregulation of HIF-2-dependent VEGF expression in the lung (4). The similarity of the phenotypes between lung epithelium-specific Akt1 TG mice and HIF-2α-deficient mice prompted us to investigate the mechanistic link between mTOR and HIF-2. Previous studies showed that mTOR enhances the transcriptional activity of HIF-1 (13) and that VEGF expression in the heart is induced by activation of the Akt-mTOR pathway in TG mice in which the Akt1 transgene is inducible in the heart by doxycycline treatment (25), suggesting that mTOR promotes HIF-1-dependent VEGF expression. However, VEGF expression in the lung was downregulated by Akt1 overexpression and restored by rapamycin treatment. Consistently, HIF-2α expression levels were downregulated in the lung of DTG mice, and reporter gene assays in cultured lung epithelial cells revealed that insulin attenuates the transcriptional activity of HIF-2 on VEGF promoter in an mTOR-dependent manner. These results suggest the possibility that HIF-2 and VEGF are situated down-

stream of mTOR in the pathogenesis of RDS and that activation of the Akt-mTOR pathway in the lung leads to RDS through the downregulation of HIF-2-dependent VEGF expression. How mTOR differentially regulates the transcriptional activity of HIF-1 and HIF-2 awaits further investigation.

There are several limitations in this study. First, because the experiments to test whether overexpression of HIF-2 or VEGF in lung epithelium rescues the RDS phenotype of Akt1 TG mice were not performed, the direct link between the Akt-mTOR pathway and the HIF-2-VEGF pathway remains to be determined. Second, although it is highly possible that hyperactivation of insulin signaling plays a causal role in RDS (8, 10, 11), the present study does not provide definitive evidence showing that insulin signaling is, indeed, activated in lung epithelium of infants having a diabetic mother. It is also possible that other factors that activate the PI3K-Akt-mTOR pathway (e.g., insulin-like growth factors) may be involved in the pathogenesis of RDS. Third, the TG mouse system used in this study may activate Akt in the lung to a supra-physiological level that is not comparable to the level of Akt activation observed in infants of diabetic mothers.

In summary, the present study demonstrates a crucial role for the Akt-mTOR pathway in the pathogenesis of infant RDS and suggests that the mTOR-HIF-2 signaling axis is a novel therapeutic target for this disease state.

ACKNOWLEDGMENTS

We thank S. L. McKnight for phEP-1, A. Ochiai and G. Ishii for A549 cells, and E. Fujita, R. Kobayashi, and Y. Ishiyama for technical assistance.

This work was supported by grants from the Ministry of Education, Culture, Sports, Science and Technology to I.K.

We declare that we have no conflicts of interest.

REFERENCES

1. **Abid, M. R., et al.** 2004. Vascular endothelial growth factor activates PI3K/Akt/forkhead signaling in endothelial cells. Arterioscler. Thromb. Vasc. Biol. **24**:294–300.
2. **Bentley-Lewis, R., S. Levkoff, A. Stuebe, and E. W. Seely.** 2008. Gestational diabetes mellitus: postpartum opportunities for the diagnosis and prevention of type 2 diabetes mellitus. Nat. Clin. Pract. Endocrinol. Metab. **4**:552–558.
3. **Clausen, T. D., et al.** 2005. Poor pregnancy outcome in women with type 2 diabetes. Diabetes Care **28**:323–328.
4. **Compernolle, V., et al.** 2002. Loss of HIF-2α and inhibition of VEGF impair fetal lung maturation, whereas treatment with VEGF prevents fatal respiratory distress in premature mice. Nat. Med. **8**:702–710.
5. **Crowther, C. A., et al.** 2005. Effect of treatment of gestational diabetes mellitus on pregnancy outcomes. N. Engl. J. Med. **352**:2477–2486.
6. **Dave, V., et al.** 2006. Calcineurin/Nfat signaling is required for perinatal lung maturation and function. J. Clin. Invest. **116**:2597–2609.
7. **Dave, V., et al.** 2008. Conditional deletion of Pten causes bronchiolar hyperplasia. Am. J. Respir. Cell Mol. Biol. **38**:337–345.
8. **Dekowski, S. A., and J. M. Snyder.** 1992. Insulin regulation of messenger ribonucleic acid for the surfactant-associated proteins in human fetal lung in vitro. Endocrinology **131**:669–676.
9. **Feig, D. S., and V. A. Palda.** 2002. Type 2 diabetes in pregnancy: a growing concern. Lancet **359**:1690–1692.
10. **Guttentag, S. H., D. S. Phelps, W. Stenzel, J. B. Warshaw, and J. Floros.** 1992. Surfactant protein A expression is delayed in fetuses of streptozotocin-treated rats. Am. J. Physiol. **262**:L489–L494.
11. **Guttentag, S. H., D. S. Phelps, J. B. Warshaw, and J. Floros.** 1992. Delayed hydrophobic surfactant protein (SP-B, SP-C) expression in fetuses of streptozotocin-treated rats. Am. J. Respir. Cell Mol. Biol. **7**:190–197.
12. **Hallman, M., V. Glumoff, and M. Ramet.** 2001. Surfactant in respiratory distress syndrome and lung injury. Comp. Biochem. Physiol. Part A **129**:287–294.
13. **Hudson, C. C., et al.** 2002. Regulation of hypoxia-inducible factor 1α expression and function by the mammalian target of rapamycin. Mol. Cell. Biol. **22**:7004–7014.
14. **Jensen, D. M., et al.** 2004. Outcomes in type 1 diabetic pregnancies: a nationwide, population-based study. Diabetes Care **27**:2819–2823.
15. **Kim, C. F., et al.** 2005. Identification of bronchioalveolar stem cells in normal lung and lung cancer. Cell **121**:823–835.
16. **Kim, H. S., et al.** 2002. Regulation of angiogenesis by glycogen synthase kinase-3β. J. Biol. Chem. **277**:41888–41896.
17. **Luukko, K., A. Ylikorkala, M. Tiainen, and T. P. Makela.** 1999. Expression of LKB1 and PTEN tumor suppressor genes during mouse embryonic development. Mech. Dev. **83**:187–190.
18. **Maemura, K., et al.** 1999. Generation of a dominant-negative mutant of endothelial PAS domain protein 1 by deletion of a potent C-terminal transactivation domain. J. Biol. Chem. **274**:31565–31570.
19. **Montan, S., and S. Arulkumaran.** 2006. Neonatal respiratory distress syndrome. Lancet **367**:1878–1879.
20. **Morimoto, M., and R. Kopan.** 2009. rtTA toxicity limits the usefulness of the SP-C-rtTA transgenic mouse. Dev. Biol. **325**:171–178.
21. **Nold, J. L., and M. K. Georgieff.** 2004. Infants of diabetic mothers. Pediatr. Clin. North Am. **51**:619–637.
22. **Northway, W. H., Jr., R. C. Rosan, and D. Y. Porter.** 1967. Pulmonary disease following respirator therapy of hyaline-membrane disease. Bronchopulmonary dysplasia. N. Engl. J. Med. **276**:357–368.
23. **Perl, A. K., S. E. Wert, A. Nagy, C. G. Lobe, and J. A. Whitsett.** 2002. Early restriction of peripheral and proximal cell lineages during formation of the lung. Proc. Natl. Acad. Sci. U. S. A. **99**:10482–10487.
24. **Shioi, T., et al.** 2003. Rapamycin attenuates load-induced cardiac hypertrophy in mice. Circulation **107**:1664–1670.
25. **Shiojima, I., et al.** 2005. Disruption of coordinated cardiac hypertrophy and angiogenesis contributes to the transition to heart failure. J. Clin. Invest. **115**:2108–2118.
26. **Shiojima, I., et al.** 2002. Akt signaling mediates postnatal heart growth in response to insulin and nutritional status. J. Biol. Chem. **277**:37670–37677.
27. **Stenmark, K. R., and S. H. Abman.** 2005. Lung vascular development: implications for the pathogenesis of bronchopulmonary dysplasia. Annu. Rev. Physiol. **67**:623–661.
28. **Taniguchi, C. M., B. Emanuelli, and C. R. Kahn.** 2006. Critical nodes in signalling pathways: insights into insulin action. Nat. Rev. Mol. Cell Biol. **7**:85–96.
29. **Tichelaar, J. W., W. Lu, and J. A. Whitsett.** 2000. Conditional expression of fibroblast growth factor-7 in the developing and mature lung. J. Biol. Chem. **275**:11858–11864.
30. **Warburton, D., et al.** 2000. The molecular basis of lung morphogenesis. Mech. Dev. **92**:55–81.
31. **Whitsett, J. A., and T. E. Weaver.** 2002. Hydrophobic surfactant proteins in lung function and disease. N. Engl. J. Med. **347**:2141–2148.
32. **Xue, Q., et al.** 2009. Rapamycin inhibition of the Akt/mTOR pathway blocks select stages of VEGF-A164-driven angiogenesis, in part by blocking S6Kinase. Arterioscler. Thromb. Vasc. Biol. **29**:1172–1178.
33. **Yanagi, S., et al.** 2007. Pten controls lung morphogenesis, bronchioalveolar stem cells, and onset of lung adenocarcinomas in mice. J. Clin. Invest. **117**:2929–2940.
34. **Zhang, Y., et al.** 2008. A Gata6-Wnt pathway required for epithelial stem cell development and airway regeneration. Nat. Genet. **40**:862–870.

Journal of Molecular and Cellular Cardiology 49 (2010) 113–120

Contents lists available at ScienceDirect

Journal of Molecular and Cellular Cardiology

journal homepage: www.elsevier.com/locate/yjmcc

Original Article

ATF6 is important under both pathological and physiological states in the heart

Hauhiro Toko [a,1], Hidehisa Takahashi [a,1], Yosuke Kayama [a], Sho Okada [a], Tohru Minamino [a], Fumio Terasaki [c], Yasushi Kitaura [c], Issei Komuro [a,b,*]

[a] Department of Cardiovascular Science and Medicine, Chiba University Graduate School of Medicine, Chiba, Japan
[b] Department of Cardiovascular Medicine, Osaka University Graduate School of Medicine, Osaka, Japan
[c] Department of Internal Medicine III, Osaka Medical College, Takatsuki, Japan

ARTICLE INFO

Article history:
Received 5 November 2009
Received in revised form 25 March 2010
Accepted 26 March 2010
Available online 7 April 2010

Keywords:
ER stress
ATF6
AEBSF
Transgenic mice
Myocardial infarction
Dominant negative
Constitutively active
Apoptosis
Bcl-2

ABSTRACT

Accumulation of unfolded proteins in the endoplasmic reticulum (ER) evokes the ER stress response, including activating transcription factor 6 (ATF6), a key transcriptional activator to maintain cellular homeostasis. The ER stress has recently been reported to cause various diseases, but the role of ATF6 in the heart remains unknown. We clarified the role of ATF6 in the heart. The ATF6 activity was increased in the murine heart after myocardial infarction (MI). Treatment of mice with 4-(2-aminoethyl) benzenesulfonyl fluoride, an inhibitor of ATF6, further reduced cardiac function and increased the mortality rate at 14 days after MI. Pharmacological inhibition of ATF6 induced dilatation of left ventricle and depression of cardiac function even in sham-operated murine hearts. The transgenic mice that expressed dominant negative mutant of ATF6 showed larger left ventricular dimension and reduced fractional shortening compared with wild-type littermates, resulting in death of heart failure at ~8 weeks of age. In contrast, cardiac function after MI was better in transgenic mice that expressed constitutively active mutant of ATF6, compared with wild-type littermates. These results suggest that activation of the ER stress response factor ATF6 plays a critical role in not only protecting hearts under the pathological state but also maintaining cardiac function under the physiological state.

1. Introduction

Newly synthesized secretory and transmembrane proteins are folded and modified in the endoplasmic reticulum (ER). A variety of extracellular stresses such as nutrient deprivation, hypoxia, oxidative stress, and calcium depletion induce accumulation of unfolded proteins in the ER [1,2], triggering the ER stress response to prevent cell death by attenuation of protein synthesis, induction of ER chaperones, and promotion of ER-associated protein degradation (ERAD) [3–5]. The quality of protein folding is monitored by ER membrane proteins, PKR-like ER kinase (PERK), activating transcription factor 6 (ATF6), and inositol requirement 1 (IRE1). Failure of these adaptive responses causes cellular dysfunction and cell death, resulting in a wide range of human disorders such as neurodegenerative diseases, inflammation and diabetes [6,7]. Targeted disruption in intestinal epithelial cells of X-box binding protein 1 (XBP1) gene, a transcription factor which undergoes unconventional splicing mediated by IRE1, has been reported to cause spontaneous colitis [8]. Abnormal long polyglutamine expansions impair ERAD [9] and cause several neurodegenerative disorders, and disruption of SIL1, a cochaperone of glucose-regulated protein 78/binding immunoglobulin protein (BiP), causes the accumulation of protein aggregates and neurodegeneration [10]. In Akita diabetic mice, mRNA levels of BiP and C/EBP homologous protein (CHOP) are increased and deletion of CHOP delays the onset of diabetes [11]. PERK null mice exhibit pancreatic β cell death and develop diabetes [12]. Furthermore, ATF6 mutation observed in Pima Indians correlates with increased susceptibility to type 2 diabetes [13]. Although it has been reported that the ER stress is increased in hypertrophic hearts [14], the precise role of the ER stress response in the heart remains unclear.

We examined the role of the ER stress response in the heart, particularly focusing on ATF6. ATF6 is a transmembrane basic leucine zipper transcription factor. In the absence of the ER stress, BiP binds to the ER luminal domain of ATF6 and inhibits ATF6 translocation from the ER to the Golgi apparatus. When the ER stress is increased, BiP dissociates from ATF6, leading to translocation of ATF6 to the Golgi apparatus. In the Golgi apparatus, ATF6 is cleaved by site-1 and site-2 proteases, and the cytoplasmic N-terminal portion of ATF6, which has a DNA-binding domain and a transcriptional activation domain, translocates to the nucleus, and activates transcription of ER-related genes such as BiP [15,16].

In this study, we clarified the role of the ER stress in the heart by examining ATF6. ATF6 was activated in the murine heart after myocardial infarction (MI). Treatment of mice with AEBSF, an

* Corresponding author. Department of Cardiovascular Science and Medicine, Chiba University Graduate School of Medicine, 1-8-1 Inohana, Chuo-ku, Chiba 260-8670, Japan. Tel.: +81 43 226 2907; fax: +81 43 226 2557.
E-mail address: komuro-tky@umin.ac.jp (I. Komuro).
[1] Contributed equally to this paper.

0022-2828/$ – see front matter © 2010 Elsevier Ltd. All rights reserved.
doi:10.1016/j.yjmcc.2010.03.020

inhibitor of ATF6, impaired cardiac function and increased the mortality rate at 14 days after MI. Furthermore, in transgenic mice, which expressed dominant negative mutant of ATF6, left ventricle was dilated and cardiac function was worse than wild-type littermates. In contrast, cardiac function after MI was better in transgenic mice, which expressed constitutively active form of ATF6, compared with wild-type littermates. These results suggest that ATF6 plays a crucial role in not only protecting cardiac remodeling under the pathological state but also maintaining cardiac function under the physiological state.

2. Materials and methods

2.1. Mice and surgical procedures

All experimental procedures were performed according to the guidelines established by Chiba University for experiments in animals and all protocols were approved by our institutional review board. We generated transgenic mice that expressed constitutively active mutant or dominant negative mutant of ATF6 in the heart [17]. A HA tag was inserted at the amino terminus just distal to the translational start site of the mutated ATF6 cDNA. The mutated cDNA was subcloned into murine α-myosin heavy chain (α-MHC) promoter-containing expression vector. The linearized DNA was injected into pronuclei of eggs from C57BL6 mice, and the eggs were transferred into the oviducts of pseudopregnant ICR mice. The transgene was identified by PCR with transgene-specific primers and by Southern blot analysis. Generation and genotyping of transgenic mice with cardiac-restricted overexpression of human Bcl-2 have been previously described [18]. The strain of Bcl-2 transgenic was mix-background between FVBN and C57BL/6. The wild-type littermates were served as controls for all studies. We anesthetized mice by intraperitoneally injecting 50 mg/kg pentobarbital sodium. Myocardial infarction (MI) was produced by ligation of the left anterior descending artery. To inhibit activation of ATF6, 4-(2-aminoethyl) benzenesulfonyl fluoride (AEBSF, 4.8 μg/g/day, Sigma, Saint Louis, MO) was continuously administered by osmotic minipump (DURECT, Cupertino, CA).

2.2. Echocardiography

Cardiac function was examined by echocardiogram (Vevo 660, VISUAL SONICS, Ontario, Canada) provided with a 25-MHz imaging transducer. All recordings were performed on conscious mice.

2.3. Histology

Hearts fixed in 10% formalin were embedded in paraffin, sectioned at 4 μm thickness, and stained with hematoxylin and eosin. For electron microscopic analysis, hearts were fixed in 4% paraformaldehyde containing 0.25% glutaraldehyde, postfixed in 1% osmium tetroxide, and embedded in Epon 812. Ultrathin sections were stained with uranyl acetate and lead citrate. For detection of apoptotic cells, TUNEL labeling was performed with an In Situ Apoptosis Detection kit (Takara, Shiga, Japan). We counted the numbers of TUNEL-positive cardiomyocytes and hematoxylin-stained nuclei in a whole section of each samples. To analyze the number of apoptotic cells in infarcted hearts, digital photographs were taken at magnification ×200, and 20 random high-power fields (HPF) from each heart samples were chosen and quantified in a blinded manner.

2.4. Western blot analysis

Whole cell lysates were resolved by SDS-polyacrylamide gel electrophoresis. Proteins were transferred onto a nitrocellulose transfer membrane (Whatman, Dassel, Germany). Western blot analysis was performed with antibodies against HA (Santa Cruz Biotechnology, Santa Cruz, CA), ATF6 (IMGENEX, San Diego, CA), BiP (Stressgen Bioreagents, Victoria, Canada), or actin (Sigma). Hybridizing bands were visualized using an ECL detection kit (GE Healthcare, Buckinghamshire, UK).

2.5. Cell culture

Cardiomyocytes were prepared from ventricles of 1-day-old Wistar rats and cultured in Dulbecco's modified Eagle's medium supplemented with 10% fetal bovine serum at 37 °C in a mixture of 95% air and 5% CO_2. Cardiomyocytes were exposed to $CoCl_2$ (100 μM, Sigma) with or without AEBSF (300 μM) for 24 h. HEK293 cells were transfected with an expression plasmid encoding mutant form of ATF6 using FuGENE6 (Roche, Indianapolis, IN). The HEK293 cells were exposed to tunicamycin (TM, 2 μg/mL, Sigma) for 6 h.

2.6. RNA extraction and quantitative RT-PCR analysis

Total RNA was isolated from the heart, neonatal cardiomyocytes or HEK293 cells with RNAZol-B (Molecular Research Center, Cincinnati, OH) according to the manufacturer's instructions. cDNA synthesis of 1 μg of RNA was carried out by using QuantiTect Reverse Transcription Kit (QIAGEN, Hilden, Germany). Quantitative real time (RT)-PCR was performed by using the LightCycler with Taqman Universal Probe Library and the Light Cycler Master (Roche).

2.7. Immunohistochemistry

Cardiomyocytes of neonatal rats cultured on glass cover slips were incubated with the antibody to α-actinin (Sigma), followed by incubation with Cy3-labeled secondary antibodies. Nuclei were counterstained with Hoechst 33258 dye. An antibody against HA was incubated with the paraffin sections of murine hearts, and immunoreactivity was evaluated using the avidin–biotin–peroxidase complex method (ScyTek Laboratories, Logan, UT). The reactions were optimized using diaminobenzidine chromogen (Vector Laboratories, Burlingame, CA) and were counterstained with hematoxylin.

2.8. Statistical analysis

Data are shown as mean ± s.e.m. Multiple group comparison was performed by one-way analysis of variance (ANOVA) followed by the Bonferroni procedure for comparison of means. Comparisons between two groups were analyzed by the two-tailed Student's *t*-test. Values of $P<0.05$ were considered statistically significant.

3. Results

3.1. ER stress response in the ischemic heart

To elucidate whether the ER stress is increased in the heart under stress conditions, we produced MI in wild-type mice. The mRNA and protein levels of BiP were increased from 1 to 4 days after MI, respectively (Fig. 1a and b). The protein levels of total (90 kDa, p90ATF6) and cleaved form (50 kDa, p50ATF6) of ATF6 and the mRNA levels of ATF6 were increased after MI (Fig. 1a and b). Furthermore, phosphorylation levels of PERK and its target protein eukaryotic initiation factor (eIF) 2α were increased at 1 and 4 days after MI, respectively (Supplemental Fig. 1a). Although phosphorylation levels of IRE1 were not significantly increased, levels of its activated form XBP1 were increased (Supplemental Fig. 1a and b). The mRNA levels of CHOP were also increased (Fig. 1b). CHOP is a transcription factor that regulates apoptosis-related factors under the ER stress condition. These results suggest that the ER stress response is induced in the heart after MI.

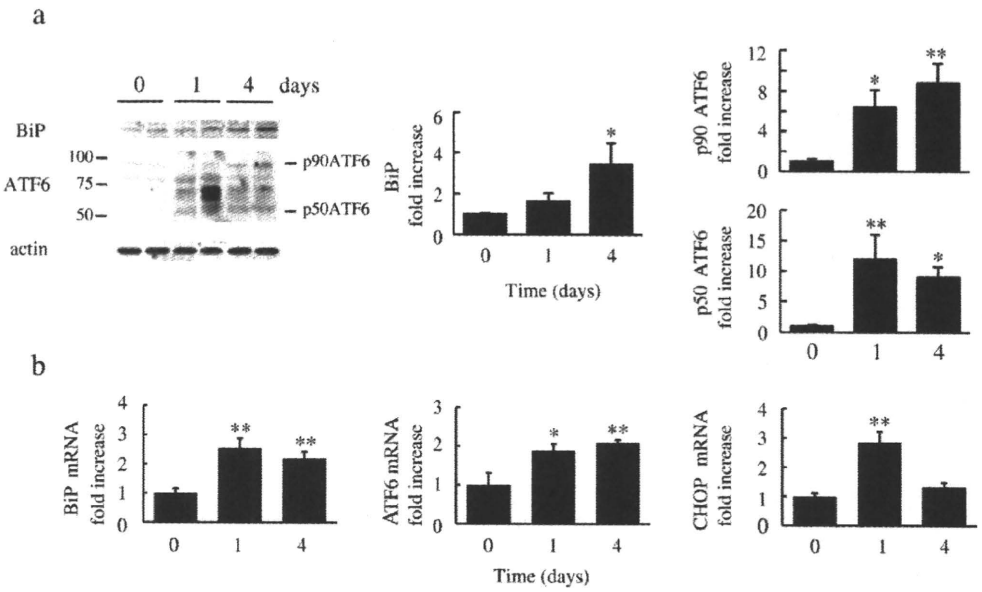

Fig. 1. ER stress response occurs in the ischemic heart. (a) Infarcted hearts during 4 days were analyzed for protein levels of BiP and total (p90ATF6) and cleaved form (p50ATF6) of ATF6 by Western blot analysis. Molecular mass makers (kDa) are indicated on the left. Quantification of BiP and ATF6 proteins as compared with sham (time = 0). $^{*}P<0.05$, $^{**}P<0.01$ versus day 0. $n=4$. (b) Expression levels of BiP, ATF6 and CHOP in hearts during 4 days of MI were quantified by RT-PCR analysis, normalized against GAPDH mRNA expression. $^{*}P<0.05$, $^{**}P<0.01$ versus day 0. $n=5$.

3.2. Inhibition of ATF6 in the ischemic heart

We examined the role of ATF6 in the ischemic heart using AEBSF, an ATF6 inhibitor [19]. We treated wild-type mice with AEBSF or vehicle and produced MI. The treatment with AEBSF was effective because it inhibited the cleavage of ATF6 (p50ATF6) in the ischemic heart (Fig. 2a). The survival rate after MI was much lower in mice treated with AEBSF than in mice treated with vehicle (Fig. 2b). In echocardiography, left ventricular posterior wall thickness was thinner, left ventricular dimension was larger and fractional shortening was smaller in mice treated with AEBSF than in mice treated with vehicle at 14 days after MI (Fig. 2c, Supplemental Table 1). These results suggest that ATF6 prevents cardiac remodeling after MI.

To clarify how AEBSF enhanced cardiac remodeling after MI, we examined expression levels of BiP, an ER chaperone which is induced by ATF6 and helps to refold unfolding proteins and ameliorates the ER stress [3,20]. mRNA levels of BiP were decreased in hearts by the treatment with AEBSF (Fig. 3a). Since it has been reported that overwhelming of the ER stress induces apoptosis, we examined apoptosis by TUNEL method. The number of TUNEL-positive cells was greater in AEBSF-treated group than in vehicle-treated group at 24 h after MI (Fig. 3b). Furthermore, expression level of CHOP was more strongly increased in AEBSF-treated group after MI (Fig. 3c). We exposed cultured cardiomyocytes to $CoCl_2$, a hypoxia mimetic, with or without AEBSF for 24 h. AEBSF augmented $CoCl_2$-induced cardiomyocyte apoptosis (Fig. 3d). To further clarify the role of ATF6 in cardiomyocytes under ischemic condition, we used a siRNA against rat ATF6. The siRNA decreased expression level of ATF6 in cardiomyocytes (Supplemental Fig. 2a), and augmented cardiomyocyte apoptosis (Supplemental Fig. 2b, lane 1 versus lane 3 and lane 5 versus lane 7). Next, we examined whether off target effects of AEBSF affect cardiomyocyte death. In the presence of the siRNA, AEBSF further increased the number of cardiomyocyte death (Supplemental Fig. 2b, lane 3 versus lane 4, lane 7 versus lane 8), suggesting that the effect of AEBSF on the heart is not only ATF6 inhibition but also some additional effects. These results suggest that inhibition of ATF6 increases ER stress-induced apoptotic death of cardiomyocytes in the ischemic heart, resulting in enhancement of cardiac remodeling after MI.

3.3. Role of dominant negative mutant of ATF6 in the heart

Pharmacological inhibition of ATF6 with AEBSF induced dilatation of left ventricle and depression of cardiac function even in sham-operated murine hearts (Fig. 2c), suggesting that ATF6 also plays a critical role in maintaining cardiac homeostasis under the physiological state. There are two forms of ATF6, ATF6α and ATF6β [21]. It has been reported that knockout mice of either ATF6α or ATF6β does not show significant phenotypes, while their double knockout mice are embryonic lethal [22,23]. Therefore, to define the role of ATF6 in the heart under the physiological state, we made transgenic mice (dnTg) that expressed a dominant negative mutant of ATF6 with HA tag under the control of α-MHC promoter (Fig. 4a) [17]. The dominant negative mutant of ATF6 has only a cytoplasmic domain of ATF6 and amino acids 315–317 of the cytoplasmic domain are changed from KNR to TAA. It has been reported that the mutant would be predicted to disrupt DNA-binding activity but dimerize with endogenous ATF6 and prevent its binding to ATF6 DNA-binding sites [17]. To confirm the effect of the mutant, we examined the expression levels of BiP in HEK293 cells transfected with the mutant. The mutant attenuated the increase of BiP expression levels by treatment of tunicamycin (TM), an ER stress inducer (Fig. 4b). Western blot analysis showed that HA was detected only in hearts of dnTg mice, and immunohistochemical analysis showed that the mutant was expressed at the nucleus of cardiomyocytes in dnTg mice (Fig. 4c). To examine whether the mutant acts as a dominant negative in vivo, we performed quantitative RT-PCR of ATF6-target genes such as BiP and ER degradation enhancing like protein 1 (EDEM1) [20,23]. The mRNA levels of BiP and EDEM1 were lower in hearts of dnTg mice compared with wild-type littermates (Fig. 4d). The survival rate was significantly lower in dnTg mice than wild-type littermates (Fig. 4e). The wall of left ventricle was thin and the cavity of hearts was dilated in dnTg mice (Fig. 4f). Echocardiographic analysis showed that left ventricular posterior wall thickness was thinner, left ventricular

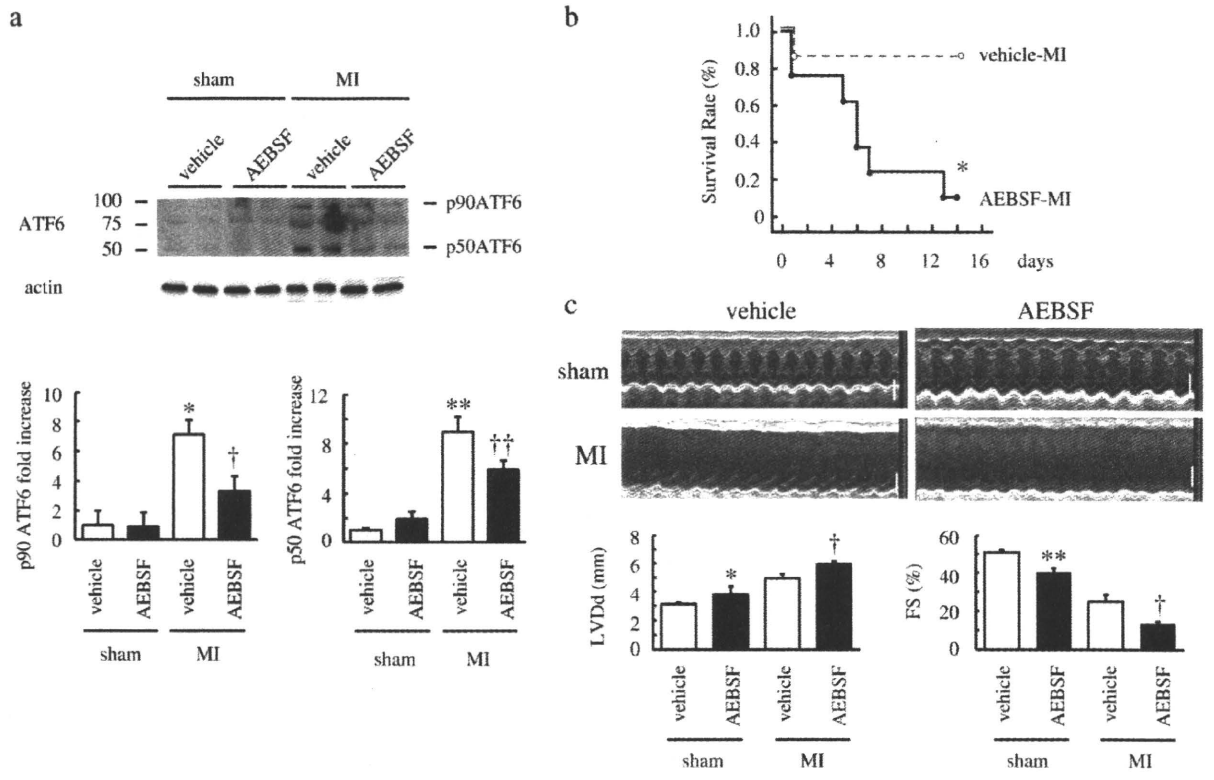

Fig. 2. AEBSF enhances cardiac remodeling after MI. (a) Sham-operated or infarcted hearts treated with vehicle or AEBSF were analyzed for protein levels of total (p90ATF6) and cleaved form (p50ATF6) of ATF6 by western blot analysis. Molecular mass makers (kDa) are indicated on the left. Quantification of ATF6 proteins as compared with sham-vehicle group. *$P<0.05$, **$P<0.01$ versus sham treated with vehicle. †$P<0.05$, ††$P<0.01$ versus MI treated with vehicle. $n=4$. (b) Kaplan–Meier survival curve after MI. *$P<0.05$ versus MI treated with vehicle. Vehicle, $n=10$; AEBSF, $n=23$. (c) Left ventricular end-diastolic dimension (LVDd) and fractional shortening (FS) were examined at 14 days after MI by echocardiogram. Scale bar, 2 mm. *$P<0.05$, **$P<0.01$ versus sham treated with vehicle. $P<0.01$ versus MI treated with vehicle.

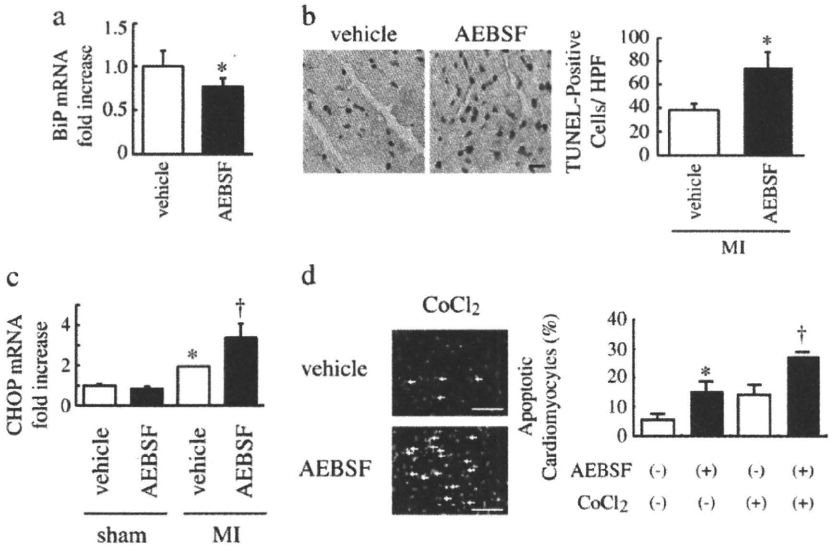

Fig. 3. AEBSF increases apoptotic cardiomyocytes. (a) Expression levels of BiP in sham-operated hearts were quantified by RT-PCR analysis, normalized against GAPDH mRNA expression. *$P<0.05$ versus vehicle. $n=5$. (b) TUNEL-positive cells (brown) in hearts at 24 h after MI. Scale bar, 10 μm. Quantitative analysis for TUNEL-positive cells at 24 h after MI. *$P<0.01$ versus vehicle. $n=4$. (c) Expression levels of CHOP in hearts of mice subjected with MI were quantified by RT-PCR analysis, normalized against GAPDH mRNA expression. *$P<0.05$ versus sham treated with vehicle. †$P<0.01$ versus MI treated with vehicle. $n=5$. (d) Cardiomyocytes were incubated with α-actinin (red), and nuclei were counterstained with Hoechst 33258 (blue). Arrows indicate condensed and Hoechst-stained nuclei indicative of apoptosis. The graph showed quantitative analysis for $CoCl_2$-induced apoptotic cardiomyocytes treated with vehicle or AEBSF. *$P<0.05$ versus non-treated cardiomyocytes. †$P<0.01$ versus $CoCl_2$-treated cardiomyocytes with vehicle. $n=5$. Scale bar, 100 μm.

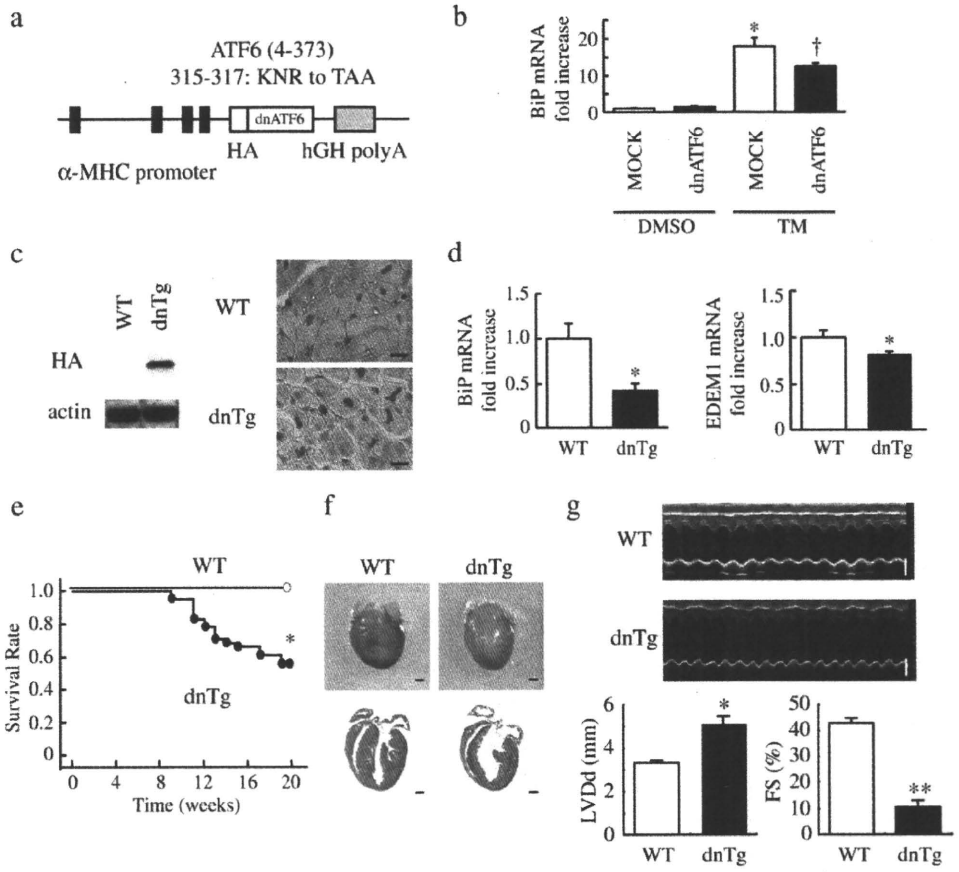

Fig. 4. The dominant negative mutant of ATF6 transgenic mice. (a) Schematic diagram represented the dominant negative mutant of ATF6 (dnATF6) transgene. HA-tagged dnATF6 was subcloned between the murine α-MHC promoter and human growth hormone (hGH) polyA. (b) Expression levels of BiP in HEK293 cells transfected with MOCK or an expression plasmid encoding the dominant negative mutant form of ATF6 were quantified by RT-PCR analysis, normalized against GAPDH mRNA expression. HEK293 cells were incubated with DMSO or TM for 6 h. *$P<0.01$ versus MOCK with DMSO, †$P<0.05$ versus MOCK with TM. $n=4$. (c) Western blot analysis and immunohistochemical staining (brown) for HA in hearts of wild-type littermates (WT) or dnTg mice at 8 weeks of age. Scale bar, 10 μm. (d) Expression levels of BiP and EDEM1 in hearts of WT or dnTg mice at 8 weeks of age were quantified by RT-PCR analysis, normalized against GAPDH mRNA expression. *$P<0.05$ versus WT. $n=4$. (e) Kaplan–Meier survival curve. *$P<0.05$ versus WT. WT, $n=19$; dnTg, $n=17$. (f) Gross morphology (upper images) and sections (lower images) of WT or dnTg murine hearts at 8 weeks of age. Scale bar, 1 mm. (g) Left ventricular end-diastolic dimension (LVDd) and fractional shortening (FS) were examined at 8 weeks of age by echocardiogram. Scale bar, 2 mm. *$P<0.05$, **$P<0.01$ versus WT.

dimension was larger and systolic function was impaired in dnTg mice compared with those in wild-type littermates (Fig. 4g, Supplemental Table 2). These results suggest that ATF6 is necessary to maintain cardiac function and structure under the physiological state.

Electron microscopic analysis showed that endoplasmic reticulums were expanded (Fig. 5a, 3 and I) and myofilaments were decreased (Fig. 5a, 4 and II) in cardiomyocytes of dnTg mice compared with wild-type littermates (Fig. 5a, 1 and 2). Expanded endoplasmic reticulums indicated that the ER stress was increased. Degenerated cardiomyocytes, suggesting apoptotic cardiomyocytes, were also observed in dnTg mice (Fig. 5a, 5 and III). Much more TUNEL-positive cardiomyocytes were observed in dnTg mice than in wild-type littermates (Fig. 5b). Furthermore, quantitative RT-PCR revealed that mRNA levels of ER stress-related apoptotic factors such as CHOP and p53 up-regulated modulator of apoptosis (PUMA) were upregulated in hearts of dnTg mice (Fig. 5c) [24,25]. To elucidate the role of cardiomyocyte apoptosis, we crossed dnTg mice and transgenic mice which overexpressed an anti-apoptotic protein Bcl-2 in cardiomyocytes [18]. Overexpression of Bcl-2 ameliorated dilatation of left ventricle and decrease of cardiac function (Fig. 5d, Supplemental Table 3), suggesting that ATF6 plays an important role in maintaining cardiac function and structure under the physiological state at least in part via inhibiting apoptosis of cardiomyocytes.

3.4. Role of constitutively active mutant of ATF6 in the heart

We next examined whether activation of ATF6 had protective effects on left ventricular remodeling after MI. Since only a cytoplasmic domain of ATF6 (aa1–373) activated expression of BiP gene (Fig. 6a) [16], we used this deletion mutant of ATF6 as a constitutively active form of ATF6. We generated transgenic mice (caTg) that expressed the cytoplasmic domain of ATF6 with HA tag under the control of α-MHC promoter (Fig. 6b) [17]. Western blot analysis showed that HA was detected only in hearts of caTg mice, and immunohistochemical analysis showed that the transgene was expressed at the nucleus of cardiomyocytes in caTg mice (Fig. 6c). There was no significant difference in heart size and cardiac function (Fig. 6d and e, Supplemental Table 4), suggesting that activation of ATF6 does not affect cardiac structure and function under the physiological state.

To examine whether activation of ATF6 had protective effects on the heart under the pathological state, we made MI in caTg mice. Echocardiographic study showed that left ventricular dimension was smaller and fractional shortening was better in caTg mice compared with in wild-type littermates at 14 days after MI (Fig. 6f). The number of TUNEL-positive cells was less in hearts of caTg mice than wild-type littermates at 24 h after MI (Fig. 6g). The survival rate was better in caTg